Article

Current Biology

A Novel Ca^{2+} Signaling Pathway Coordinates Environmental Phosphorus Sensing and Nitrogen Metabolism in Marine Diatoms

Graphical Abstract

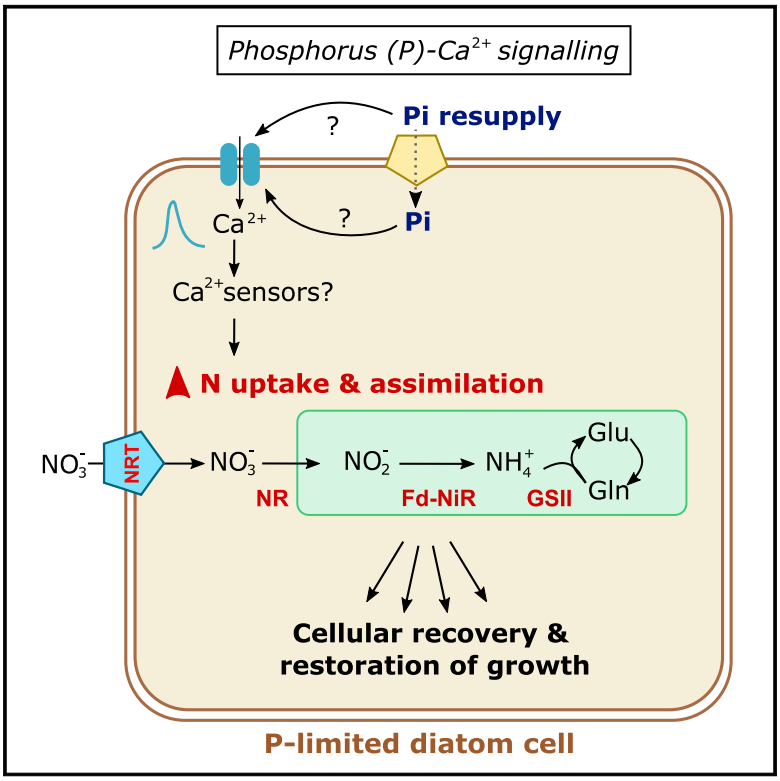

Authors

Katherine E. Helliwell, Ellen L. Harrison, Joseph A. Christie-Oleza, ..., Lisa Al-Moosawi, Colin Brownlee, Glen L. Wheeler

Correspondence

k.helliwell@exeter.ac.uk, katherine.helliwell@mba.ac.uk

In Brief

Diatoms respond rapidly to increased availability of nutrients, such as phosphorus (P) and nitrogen (N), yet little is known of diatom nutrient perception mechanisms. Helliwell et al. show that diatoms sense and coordinate rapid responses to P resupply via a Ca^{2+}-dependent signaling pathway, which drives cross-talk between P and N metabolism.

Highlights

- Phosphorus (P)-limited diatoms sense P via a Ca^{2+}-dependent signaling pathway
- P-Ca^{2+} signaling is employed by representative centric and pennate diatom species
- Rapid cross-talk with N metabolism mediates diatom recovery responses to P resupply
- P-Ca^{2+} signaling coordinates diatom recovery responses from P limitation

Helliwell et al., 2021, Current Biology *31*, 978–989
March 8, 2021
https://doi.org/10.1016/j.cub.2020.11.073

CellPress

CellPress
OPEN ACCESS

Current Biology

Article

A Novel Ca^{2+} Signaling Pathway Coordinates Environmental Phosphorus Sensing and Nitrogen Metabolism in Marine Diatoms

Katherine E. Helliwell,[1,2,6,*] Ellen L. Harrison,[1] Joseph A. Christie-Oleza,[3] Andrew P. Rees,[4] Friedrich H. Kleiner,[1] Trupti Gaikwad,[1] Joshua Downe,[1] Maria M. Aguilo-Ferretjans,[3] Lisa Al-Moosawi,[4] Colin Brownlee,[1,5] and Glen L. Wheeler[1]

[1]Marine Biological Association, The Laboratory, Citadel Hill, Plymouth PL1 2PB, UK
[2]Biosciences, College of Life and Environmental Sciences, University of Exeter, Exeter EX4 4QD, UK
[3]School of Life Sciences, University of Warwick, Warwick CV4 7AL, UK
[4]Plymouth Marine Laboratory, Plymouth, Devon PL1 3DH, UK
[5]School of Ocean and Earth Science, University of Southampton, Southampton SO14 3ZH, UK
[6]Lead Contact
*Correspondence: katherine.helliwell@mba.ac.uk or k.helliwell@exeter.ac.uk
https://doi.org/10.1016/j.cub.2020.11.073

SUMMARY

Diatoms are a diverse and globally important phytoplankton group, responsible for an estimated 20% of carbon fixation on Earth. They frequently form spatially extensive phytoplankton blooms, responding rapidly to increased availability of nutrients, including phosphorus (P) and nitrogen (N). Although it is well established that diatoms are common first responders to nutrient influxes in aquatic ecosystems, little is known of the sensory mechanisms that they employ for nutrient perception. Here, we show that P-limited diatoms use a Ca^{2+}-dependent signaling pathway, not previously described in eukaryotes, to sense and respond to the critical macronutrient P. We demonstrate that P-Ca^{2+} signaling is conserved between a representative pennate (*Phaeodactylum tricornutum*) and centric (*Thalassiosira pseudonana*) diatom. Moreover, this pathway is ecologically relevant, being sensitive to sub-micromolar concentrations of inorganic phosphate and a range of environmentally abundant P forms. Notably, we show that diatom recovery from P limitation requires rapid and substantial increases in N assimilation and demonstrate that this process is dependent on P-Ca^{2+} signaling. P-Ca^{2+} signaling thus governs the capacity of diatoms to rapidly sense and respond to P resupply, mediating fundamental cross-talk between the vital nutrients P and N and maximizing diatom resource competition in regions of pulsed nutrient supply.

INTRODUCTION

Marine phytoplankton contribute almost half of global primary production and are a major sink for rising atmospheric CO_2.[1] Diatoms are a critically important phytoplankton group, accounting for approximately 40% of organic carbon exported to the ocean interior.[2] A key attribute contributing to the environmental significance of diatoms is their ability to form spatially extensive algal blooms.[3] Diatoms frequently dominate the primary phase of spring blooms, outcompeting other phytoplankton taxa by rapidly responding to environmental cues, including increased nutrient availability.[3] In coastal systems, where diatoms thrive, nutrient supply can vary dramatically over diverse spatiotemporal scales, e.g., due to riverine inputs, turbulent mixing, upwelling, or microscale cell lysis processes.[4–6] The ability of diatoms to dominate phytoplankton assemblages in such regions of pulsed nutrient supply suggests that they possess sophisticated mechanisms for nutrient sensing. However, the sensory mechanisms enabling diatoms to rapidly respond to nutrient resupply remain poorly understood.

Phosphorus (P) is a major factor controlling ocean productivity.[7] Limitation by this nutrient is documented in a variety of marine environments,[8,9] including coastal ecosystems.[10] This has been exacerbated by anthropogenic activities causing shifts from nitrogen (N) to P limitation in certain coastal waters.[11] Certainly, bloom simulation experiments have demonstrated the importance of phosphate in controlling bloom dynamics.[12,13] Additionally, in highly productive photic benthic biofilms, the distribution of phosphate can be patchy.[14] The selective chemotaxis of diatoms toward phosphate (but not nitrate)[15] suggests phosphate may be an important driver of biofilm community structure too.

Diatoms show numerous adaptive strategies for coping with P limitation. Upregulation of phosphate transporters is well documented.[16] Moreover, enhanced expression of alkaline phosphatases and/or phosphodiesterases, increases P scavenging capacity.[16–21] Diatoms also substitute phospholipids with non-P forms to decrease cellular demand.[22,23] A transcriptional regulator, distantly related to phosphate starvation regulator protein (PSR1) of *Chlamydomonas*,[24] was recently found to coordinate such metabolic adaptations in diatoms.[25] However, these studies primarily focus on mechanisms underpinning P limitation responses.

Comparatively little is known about the short-term recovery responses of P-limited diatom cells to resupply and how they are regulated. Certainly, lipid remodeling occurs within just one cell division following phosphate amendment in *Thalassiosira*.[23] Yet the sensory systems coordinating rapid cellular recovery to newly available phosphate in diatoms are completely unknown. As these mechanisms likely underpin competitive bloom dynamics, this represents a major knowledge gap.

New insights into nutrient perception mechanisms in other eukaryotes are emerging. Vascular plants use the versatile second messenger Ca^{2+} for sensing nitrate[26,27] and K^+.[28] For instance, nitrate resupply to N-limited *Arabidopsis* plants induces $[Ca^{2+}]_{cyt}$ elevations, which triggers several nitrate-associated regulatory responses, orchestrated via Ca^{2+}-dependent protein kinases.[26] However, although Ca^{2+}-signaling mechanisms have been identified for sensing several nutrients in eukaryotes, a role for Ca^{2+} in phosphate sensing has not been reported. The work described raises important questions about the role of Ca^{2+} signaling in nutrient sensing in eukaryotes more broadly. Certainly, diatoms use Ca^{2+} signaling for perception of several abiotic and biotic stimuli.[29–31] Moreover, our recent identification of a novel class of voltage-gated channels in diatoms (EukCatAs) demonstrates that they have evolved unique mechanisms for environmental perception in the oceans.[31] Here, we report the discovery of a P-Ca^{2+}-signaling pathway that is essential for P sensing and acclimation in P limited diatoms.

RESULTS

Discovery of a P-Ca^{2+} Signaling Mechanism for Sensing Phosphate Resupply

To investigate the role of Ca^{2+} signaling in nutrient sensing in diatoms, we used a transgenic *Phaeodactylum tricornutum* line (PtR1), encoding the genetically encoded fluorescent Ca^{2+} biosensor, R-GECO1.[31,32] This Ca^{2+} reporter offers heightened sensitivity[33] and single-cell resolution compared to aequorin that has been used previously in *P. tricornutum*.[29] PtR1 cells were grown in f/2 medium[34,35] made up in natural seawater (NSW) but with reduced concentrations of phosphate, nitrate, or f/2 trace metals (STAR Methods). We then monitored single-cell R-GECO1 fluorescence of nutrient deplete cells following resupply with each respective nutrient. We observed that cells grown in phosphate-limited conditions (1.8 μM) for 4 days exhibited rapid, transient elevations in cytosolic Ca^{2+} following perfusion with seawater containing phosphate restored to 36 μM (29 out of 33 cells exhibited an increase in F/F_0 fluorescence above a threshold value of 1.15; Figures 1A and 1B). No such response was detected in phosphate-replete cells. Nor did we detect Ca^{2+} elevations in cells grown with limiting nitrate, or f/2 metals, following resupply with these nutrients (Figures 1C and S1). These data suggest that a specific Ca^{2+}-signaling pathway, which is activated only under P limitation, may be involved in regulating rapid cellular acclimation to phosphate resupply. By comparison, we found no evidence for a role for Ca^{2+} signaling in sensing nitrate (or trace metals), which is distinct from what has been observed in plants.[26]

As only P-limited cells exhibited $[Ca^{2+}]_{cyt}$ elevations following phosphate resupply, we examined further the relationship between P depletion and phosphate-Ca^{2+} signaling. We grew PtR1 cells in different phosphate regimes: (1) phosphate replete ($P_{replete}$) (36 μM); (2) phosphate limited ($P_{limited}$) (1.8 μM); or (3) no phosphate amendment (P_0) over 11 days (Figure 1D). We observed that exogenous phosphate concentrations in the medium decreased from 1.8 μM to 0.1 μM within just 2 days in $P_{limited}$ cells (initial concentrations in P_0 [NSW] medium were already very low, at 0.2 μM; Figure 1E, inset). Furthermore, growth of cells in P_0 and $P_{limited}$ treatments was significantly impaired compared to $P_{replete}$ conditions after 3 and 4 days, respectively (Figure 1D). Similarly, Fv/Fm values (a measure of the efficiency of Photosystem II)[36] were also reduced in the low P treatments (Figure S2A). Phosphate resupply experiments at different time points revealed that, after just 1 day of growth in P_0 conditions, cells exhibited the phosphate-Ca^{2+} signaling response following phosphate resupply (Figure 1E). Maximal amplitude of the response was exhibited on day 2 and gradually decreased at subsequent time points. By comparison, $P_{limited}$ cells exhibited the response after 4 days, when cell division slowed (Figure 1D). We did not detect phosphate-Ca^{2+} signaling in $P_{replete}$ cells at any of the time points. Thus, only *P. tricornutum* cells experiencing phosphate limitation exhibit phosphate-induced Ca^{2+}-signaling responses.

The P-Ca^{2+} Signaling Response Is Sensitive to Environmentally Relevant Concentrations and Forms of P

Ambient phosphate concentrations can vary significantly in coastal waters. Levels in the Western English Channel, where diatom blooms are seen frequently, can reach ~0.8 μM in February/March to lower than 0.05 μM in July.[37] Transitory spikes up to 0.97 μM during summer phosphate concentration minima likely due to mixing and/or riverine inputs have also been reported,[5] providing phosphate resupply opportunities in P-limited phytoplankton populations. To determine the sensitivity of the phosphate-Ca^{2+} signaling response, we carried out a dose-response experiment. Exposure of 4-day $P_{limited}$ PtR1 cells to resupply revealed that cells responded to environmentally relevant phosphate concentrations as low as 0.9 μM (Figure 2A). Our control condition (artificial seawater [ASW] without phosphate) did not induce a response. The described phosphate-Ca^{2+} signaling pathway thus exhibits high sensitivity to inorganic phosphate concentrations within the range of those seen in natural ecosystems.

P in the oceans can exist in numerous forms. This includes both inorganic (e.g., phosphate and polyphosphate) and organic forms. Dissolved organic phosphorus (DOP) can exceed orthophosphate concentrations,[38,39] with phosphoesters often the dominant class.[40] We tested the efficacy of different P forms for activating the Ca^{2+}-signaling response in 4-day $P_{limited}$ PtR1 cells. Treatment with equimolar concentrations (36 μM) of phosphomonoesters (adenosine triphosphate [ATP] and D-glucose-6-phosphate [G6P]) or inorganic polyP all led to transient elevations in cytosolic Ca^{2+}, similar to those evoked by phosphate (Figure 2B). In contrast, the phosphodiester bis(*p*-nitrophenyl)-phosphate (b-NPP) did not. We found that *P. tricornutum* can grow unimpaired on all of the different P forms examined, albeit at a significantly reduced specific growth rate with b-NPP (Figure 2C). These results indicate that exposure of $P_{limited}$ cells to P forms besides phosphate (with the exception of b-NPP) can evoke $[Ca^{2+}]_{cyt}$ elevations. However, it is unclear whether this

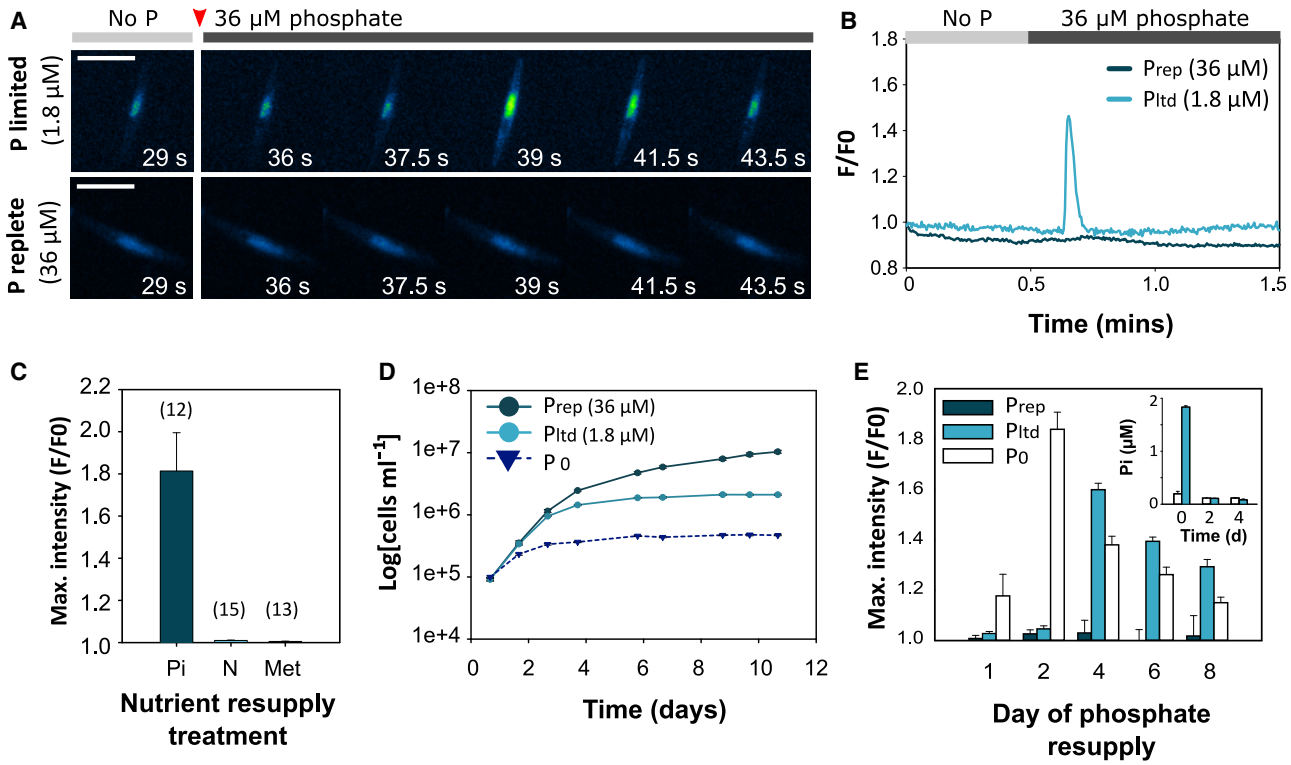

Figure 1. Increases in Environmental Phosphate Levels Trigger Rapid $[Ca^{2+}]_{cyt}$ Elevations in P-Limited *Phaeodactylum tricornutum* Cells

(A) Time-lapse images of PtR1 *P. tricornutum* cells grown for 4 days in f/2 medium in natural seawater (NSW) in either phosphate-limited (1.8 µM) or phosphate-replete (36 µM) conditions, following resupply with phosphate (36 µM). Cells were pre-perfused with standard NSW f/2 medium without phosphate for 30 s prior to perfusion with f/2 medium (including 36 µM phosphate). Time stamps indicate the time (s) from the beginning of the perfusion experiment; scale bar: 10 µm. An image of the cell just prior to phosphate resupply (i.e., at 29 s) is shown (left). The initial signal represents chloroplast auto-fluorescence. The experiment was conducted at least three times on independent samples (with a minimum of n = 8 cells examined in total) with similar results.

(B) Representative fluorescence traces of PtR1 cells for the experiment shown in (A), where F/F_0 represents the change in fluorescence intensity of R-GECO1, calculated by normalizing the fluorescence intensity of each frame by the initial value (F/F_0).

(C) Mean maximal fluorescence (F/F_0) of PtR1 cells grown for 4 days with limiting concentrations of either phosphate (1.8 µM), nitrate (44 µM), or (0 µM) of metals (Met) (Figure S1; STAR Methods), exposed to NSW with phosphate, nitrate, or Met restored to full f/2 concentrations.[34,35] Cells were pre-perfused with seawater for 30 s prior to nutrient amendments. Number (n) of cells examined over 3 independent replicate experiments carried out with a different sample of cells for each replicate is shown in parentheses above each bar; error bars represent SEM.

(D) Growth over time of PtR1 cells in standard f/2 medium with phosphate-replete ($P_{replete}$) (36 µM), phosphate-limited ($P_{limited}$) (1.8 µM), or no phosphate amendment (P_0) conditions (n = 3; Mean ±SEM; note the error bars are smaller than the markers on the plot).

(E) Mean (±SEM) maximal fluorescence (F/F_0) of PtR1 cells grown in different concentrations of phosphate over 8 days (including $P_{replete}$, $P_{limited}$, and P_0 treatments with 36 µM, 1.8 µM, and 0 µM of phosphate for each treatment, respectively), following phosphate resupply (with 36 µM). Three independent replicates each with a different sample of cells were set up per treatment, with a sample of $n \geq 6$ cells examined per independent replicate. Inset displays the concentration of phosphate (Pi) measured in the external medium for P_0 and $P_{limited}$ cells after 0, 2, and 4 days (mean ± SEM; n = 3).

See also Figures S1 and S2.

is because the P-Ca^{2+} signaling pathway can perceive these forms directly or whether phosphoesterases convert them to inorganic phosphate prior to detection. Extracellular ATP is also a well-known signaling molecule in plants and animals, which can trigger Ca^{2+}-dependent signaling pathways, regardless of P status.[41] We therefore tested the efficacy of these compounds on $P_{replete}$ cells. We did not detect Ca^{2+} elevations in response to any of these P forms in $P_{replete}$ cells (Figure 2D). Moreover, treatment of 4-day $P_{limited}$ cells with a poorly hydrolysable form of ATP, adenosine 5′-(3-thiotriphosphate) (ATP-γ-S),[42] did not yield $[Ca^{2+}]_{cyt}$ elevations (Figure 2E).

Although these results do not exclude the possibility that different P forms can directly trigger the P-Ca^{2+} signaling pathway, they strongly suggest that phosphate-starved *P. tricornutum* cells can rapidly liberate phosphate from organic P forms (likely via extracellular phosphatases),[16,21,43] which subsequently evoke a Ca^{2+} response. This is further supported by our evidence that b-NPP did not evoke a $[Ca^{2+}]_{cyt}$ elevation. Hydrolysis rates are reportedly considerably slower for b-NPP than for phosphomonoesters in *P. tricornutum*.[44] Thus, longer term processes appear to be necessary to liberate b-NPP, as is supported by the reduced growth rate of *P. tricornutum* on this substrate (Figure 2C). Taken together, these data indicate that P-Ca^{2+} signaling can be evoked, albeit indirectly, via a range of environmentally abundant P forms.

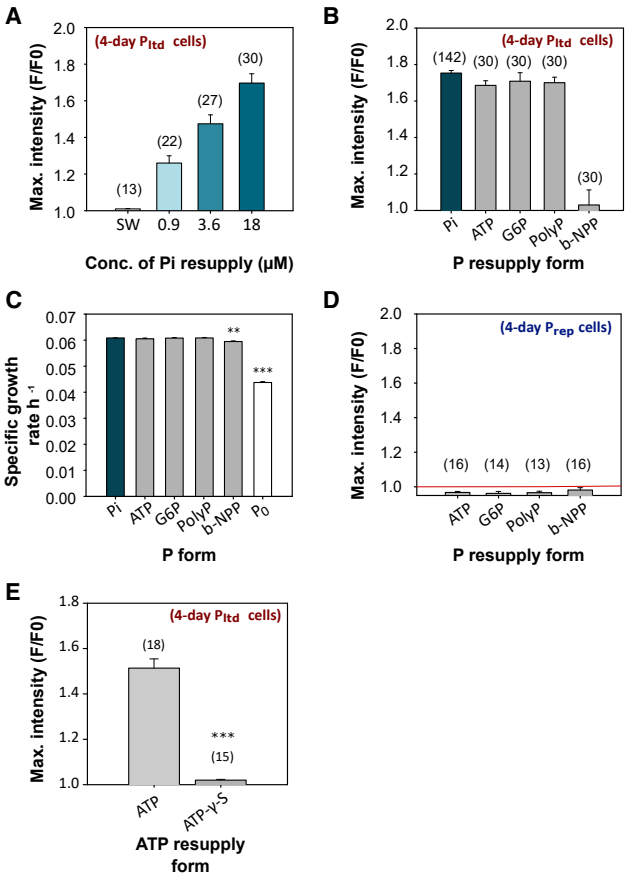

Figure 2. The P-Ca^{2+} Signaling Response Is Sensitive to Environmentally Relevant Concentrations and P Forms

(A) Maximal intensity (F/F_0) of PtR1 cells grown in $P_{limited}$ conditions with 1.8 μM phosphate for 4 days following resupply with different concentrations of phosphate (note cells were grown on NSW, but artificial seawater [ASW] was used for the phosphate resupply experiments to abolish additive effects from ambient phosphate in NSW). Prior to resupply, cells were pre-perfused for 15 s with ASW medium without phosphate or other nutrients. Cells (n) examined over 3 independent experiments each with a different sample of cells are shown in parentheses above each bar (mean ± SEM).

(B) Maximal intensity (F/F_0) of PtR1 cells grown in $P_{limited}$ conditions with 1.8 μM phosphate for 4 days following resupply with 36 μM of different P forms, including phosphate (Pi), adenine triphosphate (ATP), D-glucose 6-phosphate (G6P), polyphosphate (PolyP), or bis(*p*-nitrophenyl)phosphate (b-NPP). Cells (n) examined over 3 independent experiments, each with a different sample of cells, are shown in parentheses above each bar (mean ± SEM).

(C) Specific growth rate (h^{-1}) of PtR1 cells grown in f/2 medium with 36 μM Pi, ATP, G6P, PolyP, or b-NPP as a P source (n = 3; mean ± SEM). Asterisks (*) indicate statistically significant differences (ANOVA; ***$p < 0.001$; **$p < 0.01$) compared to the phosphate control.

(D) Mean maximal fluorescence (F/F_0) of PtR1 cells grown for 4 days in standard f/2 medium (i.e., $P_{replete}$ conditions) in response to f/2 medium without inorganic phosphate but amended with 36 μM ATP, G6P, PolyP, or b-NPP. Cells were pre-perfused with standard f/2 (natural seawater) medium without phosphate for 30 s prior to perfusion with f/2 medium (including 36 μM of the P form being tested). Number (n) of cells examined over 3 independent replicate experiments is shown; error bars represent SEM.

(E) Comparison of maximal fluorescence (F/F_0) response of 4-day old, $P_{limited}$ cells in response to 36 μM ATP versus the poorly hydrolyzable ATP-γ-S form. Number (n) of cells examined over 3 independent replicate experiments is shown using a different sample of cells for each replicate in parentheses above each bar; error bars represent SEM (Student's t test: ***$p < 0.001$).

P-Ca^{2+} Signaling Is Also Exhibited by the Ecologically Abundant Bloom-Forming Centric Diatom, *Thalassiosira pseudonana*

We have demonstrated that P-limited cells of the model pennate diatom *P. tricornutum* can detect environmentally relevant concentrations and forms of P via a previously undescribed Ca^{2+}-signaling pathway. However, diatoms represent one of the most diverse groups of algae comprising two major lineages, including the pennate (e.g., *P. tricornutum*) and centric species (e.g., *T. pseudonana*[45]).[46] We therefore wanted to investigate whether centric diatoms also employ P-Ca^{2+} signaling. We generated a transgenic strain of *T. pseudonana* expressing R-GECO1 (TpR1) (Figure 3A). Unlike *P. tricornutum*, we found that not all (only 57% of) cells within the clonal population exhibited R-GECO1 fluorescence (Figure 3A; STAR Methods). To test the ability of the R-GECO1 line to report intracellular Ca^{2+} levels, we exposed TpR1 cells to a hypo-osmotic shock treatment, which is known to induce substantial increases in cytosolic Ca^{2+} in *P. tricornutum*.[29,31] We observed large Ca^{2+} elevations in response to a 50% hypo-osmotic shock (34%; 14 out of the 41 cells examined in total; Figure 3B). Moreover, elevations were only observed in those cells clearly exhibiting R-GECO1 fluorescence prior to the shock, suggesting that the absence of response in many cells was due to poor R-GECO1 expression. To examine whether TpR1 cells exhibit P-Ca^{2+} signaling in response to P resupply, we grew cells for 4 days in standard f/2 NSW media with limiting concentrations (0.9 μM) of phosphate. Resupply of 36 μM phosphate to P-limited TpR1 cells led to transient elevations in intracellular Ca^{2+} (32%; 10 out of the total of 31 cells examined; Figure 3C; STAR Methods), albeit maximal increases in fluorescence intensity (F/F_0) were significantly lower (Student's t test; $p < 0.05$) than those seen for the 50% hypo-osmotic treatment (1.4 ± 0.06 SEM, n = 14 versus 1.2 ± 0.02 SEM, n = 10, respectively; Figure 3B). Notably, similar to *P. tricornutum*, no such response was observed in P replete cells (0/63 of cells responded to P resupply; Figure 3C). These findings demonstrate that P-Ca^{2+} signaling is present in a representative pennate (*P. tricornutum*) and centric (*T. pseudonana*) species.

Rapid Cross-Talk between P and N Metabolism Following Phosphate Resupply Revealed by Comparative Proteomics and Stable-Isotope Tracer Experiments

To determine how the P-Ca^{2+} signaling pathway regulates cellular acclimation to phosphate amendment, we employed a comparative proteomics approach to identify early recovery responses from P limitation in *P. tricornutum* following phosphate resupply. Whereas previous studies have examined longer term changes in gene expression (e.g., after 4 days) following P resupply in *P. tricornutum*,[16] we detected significant improvements in the growth rate of $P_{limited}$ cells just 24 h following phosphate resupply (Figures S2B and S2C). We therefore sought to examine shorter term proteomic responses occurring within hours of P addback. We grew PtR1 cells in $P_{replete}$ (3 × cultures) and $P_{limited}$ treatments (6 × cultures) for 4 days. We then resupplied 36 μM phosphate to three of the $P_{limited}$ cultures (for the "$P_{resupply}$" treatment) and harvested all cultures 4 h later. Total proteins were then extracted for comparative proteomics analysis. From the 1,505 identified proteins (Data S1), 443 were

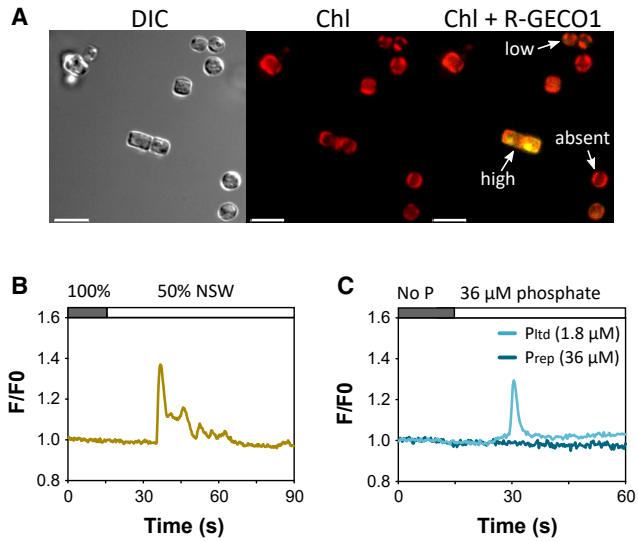

Figure 3. P-Ca^{2+} Signaling Is Also Exhibited by the Ecologically Abundant Bloom-Forming Centric Diatom, *Thalassiosira pseudonana*

(A) Epifluorescence microscope image of *T. pseudonana* TpR1 cells demonstrating R-GECO1 fluorescence in the cytosol (yellow), along with chlorophyll auto-fluorescence (red). Cells exhibiting high, low, and no detectable (absent) R-GECO1 fluorescence were observed in the clonal TpR1 line. A differential interference contrast (DIC) image is also displayed (left). Scale bar: 10 μm.

(B) Representative fluorescence trace (F/F_0) of a TpR1 cell showing increases in intracellular Ca^{2+} levels in response to 50% hypo-osmotic shock. Cells grown for 4 days in f/2 medium (made up with NSW) were pre-perfused with 100% NSW for 15 s, prior to perfusion with NSW diluted 50% with ddH_2O. The experiment was carried out on three independent occasions with a different sample of cells, and a total of 14/41 cells responded in this manner (with an increase in F/F_0 fluorescence $\geq$ 1.15).

(C) Representative fluorescence trace (F/F_0) of TpR1 cells grown for 4 days in (1) $P_{limited}$ (containing 0.9 μM phosphate; light blue line) or (2) $P_{replete}$ conditions (with 36 μM phosphate; dark blue line) in response to resupply with 36 μM phosphate. Cells were pre-perfused with 100% NSW without nutrients for 15 s, prior to perfusion with NSW + 36 μM phosphate. A total of 10/31 $P_{limited}$ cells showed an increase in F/F_0 fluorescence $\geq$ 1.15, compared to 0/61 of $P_{replete}$ cells, over three independent experiments.

differentially expressed (exhibiting a log2 fold change $\geq$ 1; ≤ -1; $Q < 0.05$) in $P_{limited}$ versus $P_{replete}$ cells (215 were more abundant and 228 were less abundant). By comparison, 232 proteins had significantly altered abundance in $P_{resupply}$ versus $P_{limited}$ cells (63 increased and 169 decreased abundance; Figure S3; Data S2 and S3). We classified differentially expressed proteins into specific metabolic pathways, using Mercator-based analyses.[47] This identified broad-scale impacts of phosphate regime on proteins associated with protein, nitrogen, DNA and RNA, cell division, photosynthesis, and signaling (Figure S3; Data S2 and S3), consistent with previous studies.[16,48]

As expected, we observed significant enhancement of putative phosphate acquisition and recycling proteins in $P_{limited}$ versus $P_{replete}$ cells.[16,18] Indeed, under P limitation, the four most highly expressed proteins included a predicted glycerophosphoryl diester phosphodiesterase and three putative alkaline phosphatases (Data S3). In the $P_{resupply}$ treatment, these proteins remained highly expressed 4 h following phosphate resupply. Notably, by comparison, some of the most significantly altered proteins in the $P_{resupply}$ treatment compared to $P_{limited}$ cells related to N uptake/assimilation. This included upregulation of a predicted nitrate transporter (NRT) that showed a striking 5.7 log2 fold increase, alongside five other N metabolism proteins (Figures 4A and 4B). These data suggest that a major immediate response to phosphate resupply in diatoms is the upregulation of N assimilation and metabolism.

To directly examine the impact of phosphate resupply on N uptake over time, we characterized changes in total cellular N content, and ^{15}N-nitrate uptake, in PtR1 cells experiencing different P regimes ($P_{replete}$, $P_{limited}$, and $P_{resupply}$). We grew $P_{replete}$ and $P_{limited}$ cultures for 4 days, as described previously for the proteomics sampling. Prior to phosphate resupply (to $P_{limited}$ cells for the $P_{resupply}$ treatment), we added ^{15}N-nitrate (to a concentration 10% of ambient nitrate) to all the cultures and acclimated cells for 1 h. We then quantified the total N content and ^{15}N enrichment (expressed as atom% ^{15}N) over 24 h following phosphate resupply. At T_0 (i.e., just prior to phosphate resupply), $P_{replete}$ cells had 2.9 times more total N than $P_{limited}$ cells (Figure 4C). However, upon phosphate resupply, significant increases in total N content were detected within just 8 h, and levels exceeding those in $P_{replete}$ cells were measured in 24 h. By comparison, the cellular N content of $P_{limited}$ cells remained low. Moreover, the increases in total N content were accompanied by approximately 9-fold increases in atom% ^{15}N levels within 24 h following phosphate resupply (Figure 4D). By comparison, the levels in $P_{limited}$ cells only increased modestly beyond initial values. Moreover, absolute nitrate uptake rates were twelve times greater in $P_{resupply}$ compared to $P_{limited}$ cultures and 1.5 times more than the $P_{replete}$ cells over 24 h (Figure 4E). These data demonstrate that the proteomic changes observed in the abundance of predicted N-transport-associated proteins, as a consequence of P resupply, result in rapid and substantial increases in N uptake.

Enhanced N Transport Is a Primary Acclimation Response Driving Recovery from P Limitation

We have observed enhanced N transport in $P_{limited}$ cells within just 8 h of phosphate amendment. N is a major constituent of proteins, nucleic acids, and chlorophyll. Alongside proteomic changes in N assimilation machinery, we observed concomitant increases in numerous proteins of protein metabolism in $P_{resupply}$ versus $P_{limited}$ cells. This included the increased abundance of 19 predicted synthesis proteins and decreased abundance of 13 putative degradation proteins (Figure S3; Data S2). We confirmed that total protein content was significantly reduced in $P_{limited}$ compared to $P_{replete}$ cells and subsequently recovered following phosphate resupply after 24 h (Figure 5A), when increases in growth rate were also detectable (Figures S2B and S2C). The abundance of 13 photosynthesis-related proteins were also altered in $P_{resupply}$ versus $P_{limited}$ cells, including four predicted light harvesting complex proteins, cytochrome B6 (PetB), and two predicted photosystem II proteins (PsbC and PsbA) that exhibited decreased abundance in the $P_{resupply}$ treatment compared to $P_{limited}$ cells (Data S2). However, the majority of predicted fucoxanthin chlorophyll a/c binding proteins detected (23/29 proteins) did not exhibit differential abundance in the $P_{resupply}$ treatment compared to $P_{limited}$ cells (log2 fold change $\geq$ 1; ≤ -1) at this time point. Certainly, we only detected

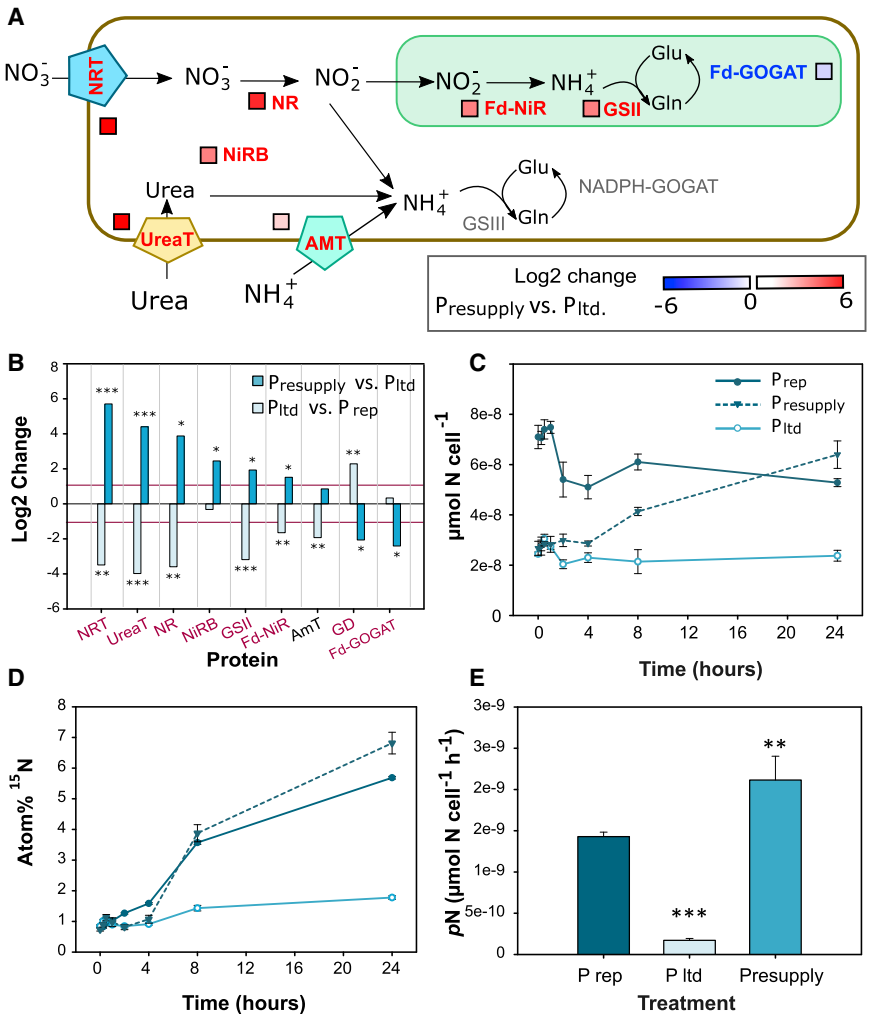

Figure 4. Rapid Cross-Talk between P and N Metabolism following Phosphate Resupply

(A) A cohort of proteins predicted to be associated with N uptake and assimilation exhibited altered abundance after 4 h in $P_{resupply}$ compared to $P_{limited}$ cells. This included increased abundance of a putative nitrate transporter (NRT) (JGI protein identifier: 26029/54101), urea transporter (UreaT) (20424/768), nitrate reductase (NR) (54983), NAD(P)H-dependent nitrite reductase (NirB) (13154), chloroplast-targeted glutamine synthetase (GSII) (51092), and ferredoxin-dependent nitrite reductase (Fd-NiR) (12902). We also saw decreased abundance of a putative glutamate dehydrogenase (GD) (45239) and the chloroplast-targeted glutamate synthase (Fd-GOGAT) (56605).

(B) Bar graph of protein fold changes of putative N metabolism proteins described in (A) in response to phosphate resupply (relative to $P_{limited}$ cells; log2 fold change $\geq$ 1; Q < 0.05 labeled purple). The log2 fold changes of proteins exhibiting significantly altered abundance in $P_{limited}$ cells relative to $P_{replete}$ cells are also shown. Asterisks (*) indicate statistically significant differences (Student's t test q-value; ***q < 0.001; **q < 0.01; *q < 0.05).

(C and D) Total N uptake (µmol N $cell^{-1}$; C) and atom% ^{15}N (D) in $P_{replete}$, $P_{limited}$, and $P_{resupply}$ treatments following phosphate resupply to P-limited cells over 24 h (mean [n = 3] ± SEM).

(E) Absolute nitrate uptake rates (pN) µmolN $cell^{-1}$ h^{-1} of $P_{replete}$, $P_{limited}$, and $P_{resupply}$ cultures following phosphate resupply to phosphate-limited cells over 24 h (mean [n = 3] ± SEM). Asterisks (*) indicate statistically significant differences (one-way ANOVA; ***p < 0.001; **p < 0.01) compared to the phosphate-replete control.

See also Figure S3 and Data S1, S2, and S3.

increases in Fv/Fm values and total chlorophyll within 24 h following P resupply (Figures 5B and 5C). Additionally, a rapid reduction in non-photochemical quenching (NPQ), a vital photo-protection mechanism, was seen 6 h following phosphate resupply (Figures 5D and 5E). Notably, the observed reductions in NPQ, which occurred on a time frame similar to the changes observed for N transport (Figures 4C and 4D), occurred concomitantly with an increase in electron transport rates (ETRs) (µmol e m^{-2} s^{-1}) of $P_{resupply}$ cells (Figure 5D, red). This could therefore serve to enhance photosynthetic reducing power to drive other vital processes, including N assimilation.

A key response of diatoms to P limitation is the accumulation of neutral lipids, including triacylglycerides (TAGs), and substitution of membrane phospholipids.[16,22] However, we detected just five proteins of lipid synthesis/metabolism exhibiting differential abundance (log2 fold change $\geq$ 1; Q < 0.05) in $P_{resupply}$ versus $P_{limited}$ cells (Data S2). This included the decreased abundance two putative fatty-acid biosynthesis enzymes: enoyl-coenzyme A (CoA) hydratase (ECH1) and acetyl-CoA carboxylase (ACC1) that catalyze the synthesis of precursors for TAG biosynthesis.[49] The downregulation of these proteins corresponded with the recovery of TAG levels to those similar to $P_{replete}$ cells, 24 h following phosphate resupply (Figure S4).

Together, our evidence demonstrates that the substantial increases in N uptake (alongside NPQ adjustments) following P resupply are among some of the first detectable metabolic responses of P-limited *P. tricornutum* cells to P amendment. These adaptations, which occur within 8 h, precede recovery of cellular protein, TAG and chlorophyll content, Fv/Fm, and growth. The primary adaptations of N metabolism thus likely underpin subsequent cellular adaptations necessary to kick-start cellular growth following phosphate amendment.

P-Ca^{2+} Signaling Is Necessary for Primary Adaptations in Nitrate Metabolism following Phosphate Resupply

We have characterized early physiological adaptations underpinning P limitation recovery and identified an important role for N uptake and NPQ adaptation within hours of phosphate resupply. However, alongside acclimation of primary metabolism, we saw increased abundance of numerous Ca^{2+}-signaling-related proteins in $P_{limited}$ versus $P_{replete}$ cells, including several Ca^{2+}/calmodulin-dependent protein kinases that could serve as sensors for phosphate-induced Ca^{2+} elevations (Data S3;

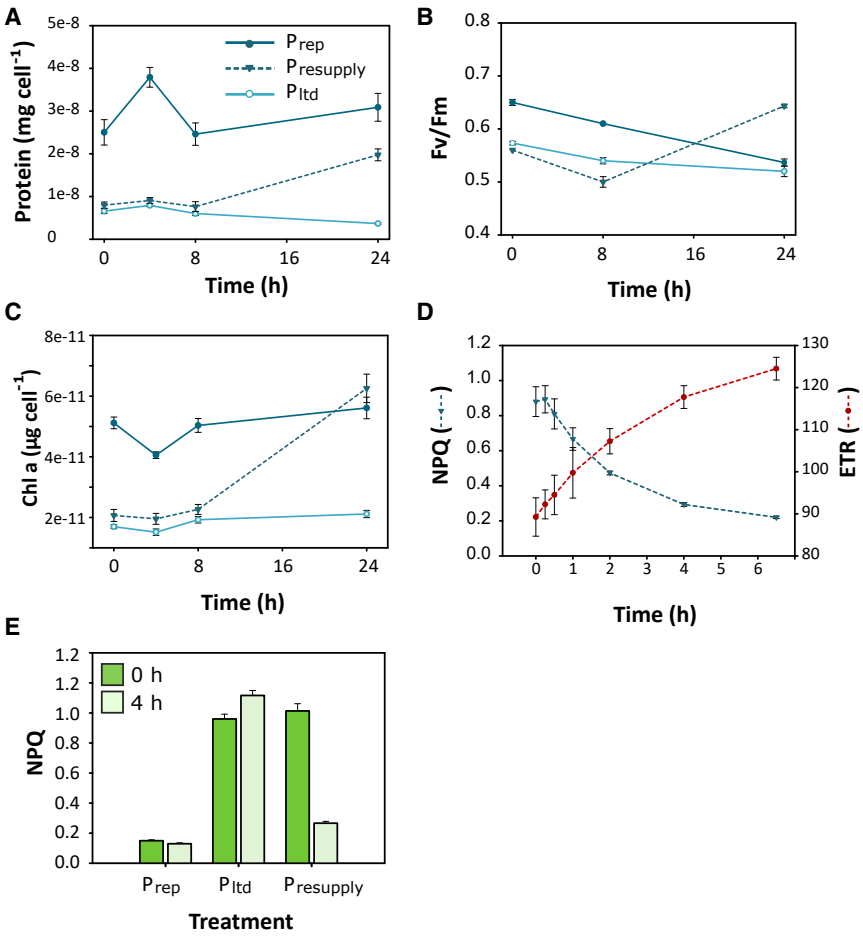

Figure 5. A Succession of Metabolic Acclimation Responses Drive Recovery from Phosphate limitation

(A–C) Changes over time of (A) total protein content (mg cell^{-1}), (B) Fv/Fm, and (C) total chlorophyll a (chl a) content (µg cell^{-1}) of P-limited ($P_{limited}$) (1.8 µM) cultures following resupply ($P_{resupply}$) of phosphate (36 µM), compared to $P_{replete}$ (36 µM) and $P_{limited}$ grown cells.

(D) Changes in non-photochemical quenching (NPQ) and electron transport rate (ETR) (µmol electrons m^{-2} s^{-1}) in $P_{limited}$ cells in response to phosphate resupply over 6 h.

(E) NPQ values of $P_{replete}$, $P_{limited}$, and $P_{resupply}$ prior to (0 h) and 4 h after phosphate resupply. All values plotted are mean (n = 3) ± SEM.

See also Figures S3 and S4.

Figure S5), as has been documented in the nitrate-Ca^{2+} signaling response of *Arabidopsis*.[26] These findings uncover putative mechanistic components of the pathway and add further evidence to the importance of Ca^{2+} signaling in P sensing and likely role in regulating metabolic adaptations to P resupply.

To examine whether the P-Ca^{2+} signaling pathway mediates downstream recovery responses from P limitation following phosphate resupply, we investigated the source of the phosphate-induced Ca^{2+} signal and its sensitivity to pharmacological inhibitors, with the aim to identify avenues to inhibit phosphate-Ca^{2+} signals. Treatment of $P_{limited}$ cells to phosphate resupply in ASW made up without Ca^{2+} (+200 µM EGTA) completely abolished the phosphate-induced Ca^{2+} elevation (Figure 6A), indicating dependency of the response on external Ca^{2+}. This suggests that plasma membrane localized Ca^{2+} channels are involved. *P. tricornutum* encodes a number of Ca^{2+} channel homologs,[50] for which there has been little/no functional characterization. This is with the exception of a novel class of channels that we recently characterized in diatoms (EukCatAs).[31] We therefore examined whether *Pteukcata1* knockout mutant lines[31] are impaired in phosphate-Ca^{2+} signaling. All lines tested evoked phosphate-induced $[Ca^{2+}]_{cyt}$ elevations comparable to PtR1 (Figure 6B), indicating that PtEUKCATA1 is not involved in the primary Ca^{2+} response to phosphate. We also adopted a pharmacological approach, testing the effect of Ca^{2+} channel blockers on phosphate-Ca^{2+} signals. These experiments revealed that, whereas pre-treatment of cells with verapamil (L-type Ca^{2+} channel inhibitor) did not disrupt the phosphate-Ca^{2+} signal (Figure S6A), 5 µM Ruthenium Red (RuR) (inhibits a range of Ca^{2+} channels)[51] inhibited the response (Figure 6C). By comparison, 5 µM RuR did not disrupt Ca^{2+} signaling responses to hypo-osmotic stress (Figures S6B and S6C). Thus, RuR does not interfere with the capacity of R-GECO1 to report Ca^{2+} or cause broad disruption of Ca^{2+} signaling processes within the cell.

We therefore investigated the effect of inhibiting the phosphate-Ca^{2+} signaling pathway on early primary adaptations (i.e., N uptake and NPQ) to phosphate amendment in $P_{limited}$ cells. We first examined the impact of RuR inhibition on the nitrate uptake response, limiting exposure of cells to RuR to 8 h. As previously observed, we saw substantial increases in atom% ^{15}N in the $P_{replete}$ treatments in the absence of RuR (Figure 6D, left). This was also the case in the presence of 5 µM RuR, albeit to a lesser extent (Figure 6D, right). These results indicate that nitrate uptake can still occur in the presence of RuR. However, we detected a significant increase in atom% ^{15}N following P resupply within 8 h, which was completely absent in P-limited cells (Figure 6D, left). By comparison, in the $P_{resupply}$ treatment +5 µM RuR, no increases in atom% ^{15}N levels were observed at all. To examine whether the altered nitrate uptake in the $P_{resupply}$ +RuR treatment was due to reduced cell health following incubation with RuR, we measured Fv/Fm values. However, exposure of $P_{resupply}$ cells to 5 µM RuR for 8 h did not reduce Fv/Fm values, compared to the −RuR control (Figure S6D). Finally, we tested the impact of RuR on NPQ under different P regimes, including following phosphate resupply (Figure S6E). The fast reductions in NPQ were still observed in the presence of RuR following P resupply (Figure S6F). Therefore, RuR-treated $P_{limited}$ cells still exhibit phosphate-induced NPQ recovery responses.

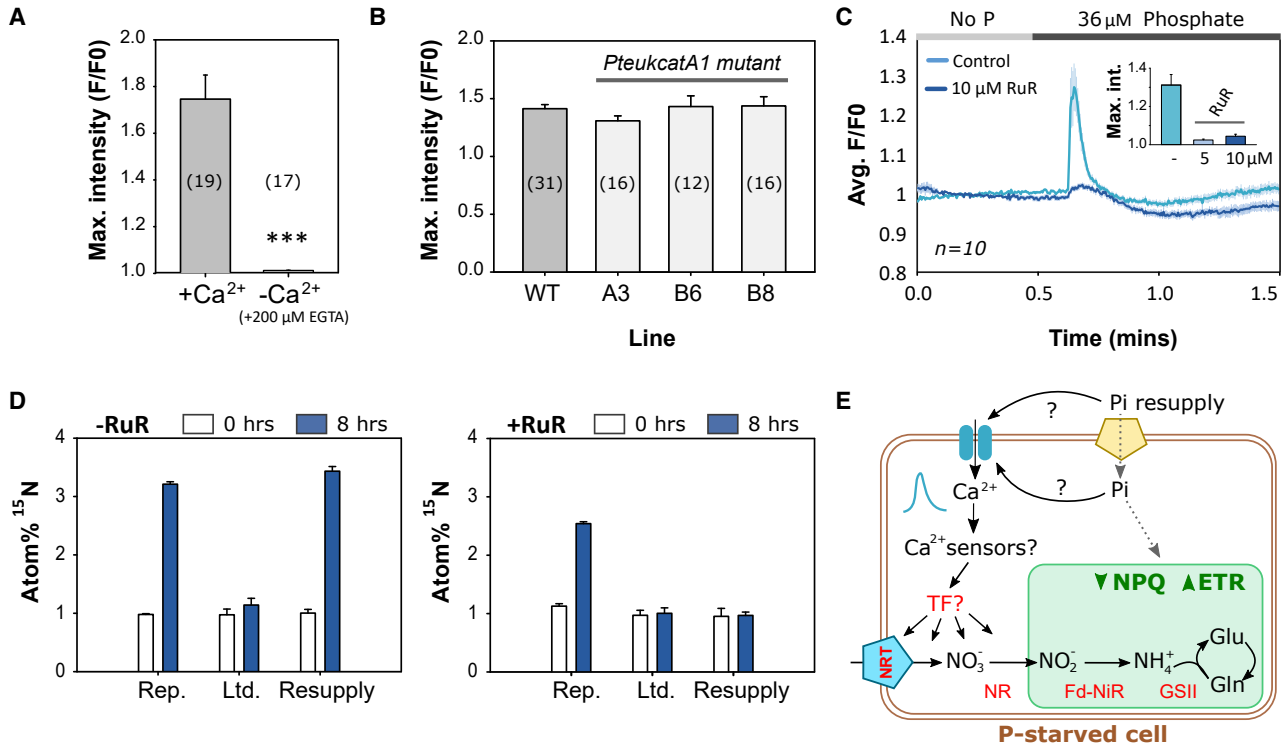

Figure 6. Phosphate-Ca^{2+} Signaling Is Necessary for Nitrate Uptake following Phosphate Resupply

(A) Average maximal fluorescence (F/F_0) of 4-day PtR1 cells grown in ASW with limited phosphate (1.8 µM) exposed to phosphate resupply (36 µM) either $+Ca^{2+}$ (in standard ASW containing 10 mM $CaCl_2$) or $-Ca^{2+}$ (in ASW without 10 mM $CaCl_2$ + 200 µM EGTA). No. of cells (n) examined over 3 independent experiments each with a different sample of cells is shown in parentheses above each bar (mean ± SEM; Student's t test; ***$p < 0.001$).

(B) Comparison of average maximal fluorescence (F/F_0) values of phosphate-Ca^{2+} signaling response in PtR1 cells versus three independent *PteukcatA1* mutant lines in a PtR1 background.[31] Cells were grown in standard f/2 medium (with NSW) with low phosphate (1.8 µM) prior to the experiment. Cells (n) examined over 3 independent experiments per line each with a different sample of cells are shown in parentheses above each bar (mean ± SEM).

(C) Average fluorescence trace of the phosphate-Ca^{2+} signaling response in PtR1 cells pre-treated for 5 min with 10 µM RuR, compared to control (no inhibitor). Prior to phosphate resupply, cells were pre-perfused for 30 s with NSW medium without RuR, phosphate, or other nutrients. Inset displays average maximal F/F_0 values of the phosphate-Ca^{2+} signaling response without inhibition (–) and following treatment with 5 µM RuR and 10 µM RuR (n = 17, 19, and 13 cells over three independent experiments; mean ± SEM).

(D) Atom% ^{15}N measured in cells under different phosphate regimes in the absence or presence of 5 µM RuR. The atom% ^{15}N measured at T = 0 (prior to phosphate resupply) and 8 h post-phosphate resupply is shown (n = 3; mean ± SEM; experiments were repeated twice with similar results).

(E) Schematic model for the P-Ca^{2+} signaling pathway. Ca^{2+}-independent components are indicated with dashed arrows (TF, transcription factor).

See also Figures S5 and S6.

Together, our findings demonstrate that the rapid changes in NPQ capacity can occur in a Ca^{2+}-independent manner, potentially responding directly to increased cellular P quotas detectable within hours following phosphate resupply in *P. tricornutum*.[52] By comparison, fundamental increases in nitrate uptake in $P_{limited}$ cells following phosphate resupply are dependent on phosphate-induced $[Ca^{2+}]_{cyt}$ elevations (Figure 6E). Thus, the P-Ca^{2+}-signaling pathway is vital for regulating primary metabolic recovery from P limitation and also serves to maximize acquisition and resource competition for the vital limiting nutrient N.

DISCUSSION

We report the discovery of a Ca^{2+} signaling pathway in diatoms to sense and rapidly respond to increases in P availability (Figure 6E). We show that the addition of phosphate to phosphate-limited diatom cells results in cytosolic Ca^{2+} elevations within seconds of resupply (Figure 1). This response was detectable in the pennate *P. tricornutum* (that exhibits both benthic and planktonic modes of life)[53] and the ecologically abundant planktonic bloom-forming centric species *T. pseudonana* (Figure 3), indicating that P-Ca^{2+} signaling is employed by evolutionarily diverse diatom taxa for P sensing. Moreover, in *P. tricornutum* the response is evoked by environmentally relevant phosphate concentrations and (indirectly) by different P forms (Figures 2A and 2B). Importantly, inhibition of P-Ca^{2+} signaling completely blocks a critical component of cellular recovery from phosphate limitation (nitrate uptake; Figure 6) that underpins subsequent physiological responses (Figure 5). Although RuR was able to block P-Ca^{2+} signaling, it did not impair the Ca^{2+}-signaling response of *P. tricornutum* to hypo-osmotic shock (Figure S6). Nevertheless, the specificity of RuR against the diatom Ca^{2+}-signaling toolbox more broadly

is not fully understood. Future work is therefore necessary to identify the specific molecular machinery underpinning the P-Ca^{2+} signaling pathway and determine how the observed cross-talk between P and N metabolism is mediated. Our study suggests that P-Ca^{2+} signaling is critical to P-limited diatom cells for sensing and rapidly responding to P resupply in dynamic nutrient environments (e.g., in upwelling and coastal systems).[5] More broadly, these findings provide much needed insight into the molecular mechanisms employed by eukaryotic algae for sensing P resupply, which until now have remained enigmatic.[20]

Importantly, our work highlights that fundamental cross-talk between the essential nutrients P and N drive ecological acclimation to P availability in diatoms. Evidence suggests that P-limited cells invest primarily in phosphate acquisition,[16,18] scavenging,[10,17] and reallocation,[23] diverting resources away from vital processes, such as N assimilation. Meanwhile, activation of the P-Ca^{2+} signaling machinery readies cells for detection of P resupply. This activation is first evident after 4 days of growth in P-limited conditions (1.8 μM phosphate; Figure 1E), even though the extracellular phosphate concentrations became fully depleted after only 2 days in this treatment. This suggests that intracellular phosphate status, rather extracellular phosphate concentrations, mediate P-Ca^{2+} signaling activation. By comparison, induction of *P. tricornutum* alkaline phosphatase was detectable when ambient phosphate concentrations were $\leq$ 3.6 μM.[54] The rapid phosphate-driven induction of N uptake and assimilation proteins allows P-limited cells to control the allocation of resources to priority cellular functions, which must then be rapidly rewired when conditions change. This rapid coordination between P and N metabolism, via the P-Ca^{2+} signaling, enables diatoms to immediately exploit another vital limiting nutrient within hours of being released from P limitation, driving enhancements in growth rate detectable within 24 h (Figures S2B and S2C). The timescale of such changes could promote the competitive ability of diatoms in regions of pulsed nutrient supply, such as upwelling ecosystems,[6] in which favorable wind conditions can drive nutrient upwelling events lasting 1 to 2 weeks.[55,56] As phosphate resupply events (e.g., due to riverine inputs, upwelling, or microscale cell lysis)[6] often occur simultaneously with enhanced nitrate abundance,[57] by upregulating N assimilation, the P-Ca^{2+} signaling pathway primes the cell to anticipate improved nutrient conditions more generally and enables the balanced acquisition of P and N. Notably, N-transport and assimilation genes are key indicators of phytoplankton N status[58] and can also exhibit rapid responsiveness to N resupply.[59] However, we found no evidence for a role of Ca^{2+} signaling in nitrate sensing in N-limited *P. tricornutum* cells (Figure 1C). Together, these data highlight that multiple environmental drivers coordinate resource-responsive gene expression in diatoms via complex regulatory networks.

From an ecological standing, the rapid draw-down of N, mediated by P-Ca^{2+} signaling, enables diatoms to adapt rapidly to acquire another major vital nutrient and enhance their ability to compete for resources in highly dynamic nutrient regimes. Certainly, evidence from the Western English Channel demonstrates that diatoms frequently outcompete other phytoplankton taxa when P supply is intermittent. Summer diatom blooms dominated by pennate diatoms have been observed in these regions in response to pulses of phosphate in the surface waters (which also co-occurred with small increases in nitrate and ammonium concentrations).[60] This provides important evidence that diatoms are particularly successful competitors under fluctuating P regimes. This ecological success must in some part be attributed to their sensory mechanisms, which enable them to rapidly respond to environmental P concentrations. Although little is known about how other eukaryotic phytoplankton sense P resupply and whether or not they also employ P-Ca^{2+} signaling, diatom P-Ca^{2+} signaling is certainly distinct from the P sensory systems characterized in other marine microbes. For instance, the marine cyanobacterium *Synechococcus* sp. WH7803 employs a two-component mechanism analogous to the PhoR-PhoB system of *Escherichia coli*.[61] In these bacterial systems, a histidine protein kinase protein (PhoR) senses P availability.[62] Under low P, PhoR activates the response regulator (PhoB), which directly binds to upstream sequences of P-responsive genes to activate P starvation responses. However, in eukaryotic diatom cells (that can range from 2 μm [e.g., *Minidiscus*] to up to 3 mm [e.g., *Ethmodiscus*] in diameter), Ca^{2+}-dependent P-sensing mechanisms likely confer several advantages. The significant electrochemical gradient for Ca^{2+} across cellular membranes allows very rapid modulation of intracellular Ca^{2+} concentrations that can span whole diatom cells within seconds. Furthermore, Ca^{2+} can rapidly and reversibly bind to numerous downstream protein targets to simultaneously modulate their conformation and activity directly.[50] These properties render Ca^{2+} signaling particularly suitable for eukaryote signal transduction pathways and may explain the evolution of distinct mechanisms for P sensing between prokaryotic and eukaryotic marine microbes.

On a final note, this study expands the portfolio of biological functions of Ca^{2+} signaling known. Diatoms are evolutionarily divergent from plants and animals, in which Ca^{2+} signaling research is well established. By broadening our study to important taxa outside of "crown" eukaryote groups, with fundamentally different ecologies, we can gain a more comprehensive understanding of the role and evolution of Ca^{2+} signaling across eukaryotes. By taking this approach, we have identified that distinct mechanisms for nutrient perception have arisen. Diatom-like P-Ca^{2+} signaling is apparently absent in plants: phosphate-induced $[Ca^{2+}]_{cyt}$ elevations were not detected in P-limited *Arabidopsis*.[63] Similarly, unlike *Arabidopsis*,[26] nitrate resupply did not evoke a Ca^{2+}-signaling response in N-limited *Phaeodactylum* cells. Nevertheless, diatom P-Ca^{2+} signaling does share features with Ca^{2+}-dependent nitrate sensing in *Arabidopsis*.[26] Both pathways coordinate expression of N-related genes via Ca^{2+}. In *Arabidopsis*, this is orchestrated by Ca^{2+} sensor kinases that phosphorylate NIN-LIKE PROTEIN (NLP) transcription factors (TFs). Intriguingly, NLP TF genes are absent from diatom genomes.[64] However, we did find four Ca^{2+} sensor-kinase genes upregulated during P limitation. Notably, these genes contain recognition motifs for the P-starvation TF, PtPSR.[25] Our work thus paves the way to future advances in our understanding of the genetic components, evolutionary distribution, and broader roles of phosphate-Ca^{2+} signaling in controlling recovery from P limitation in diatoms and potentially eukaryotes more broadly.

STAR★METHODS

Detailed methods are provided in the online version of this paper and include the following:

- KEY RESOURCES TABLE
- RESOURCE AVAILABILITY
  - Lead Contact
  - Materials Availability
  - Data and Code availability
- EXPERIMENTAL MODEL AND SUBJECT DETAILS
  - Strains and cultivation of *P. tricornutum* and *T. pseudonana*
- METHOD DETAILS
  - Generation of *T. pseudonana* R-GECO1 constructs
  - Biolistic transformation of *T. pseudonana*
  - Epifluorescence imaging in *P. tricornutum* and *T. pseudonana*
  - Treatment with pharmacological inhibitors for Ca^{2+}-signaling experiments
  - Protein preparation for shotgun proteomics
  - NanoLC-MS/MS and data analysis of the proteomes
  - Biochemical analyses
- QUANTIFICATION AND STATISTICAL ANALYSIS
  - Statistical Analyses
  - Data and Software Availability

SUPPLEMENTAL INFORMATION

Supplemental Information can be found online at https://doi.org/10.1016/j.cub.2020.11.073.

ACKNOWLEDGMENTS

We acknowledge support from the NERC-IRF grants NE/R015449/2 (K.E.H.) and NE/K009044/1 (J.C.-O.), ERC grant ERC-ADG-670390 (C.B.), and the NERC-CLASS program grant (NE/R015953/1; A.P.R.). We are also grateful to the Proteomics Research Technology Platform (University of Warwick, UK) and Malcolm Woodward (PML, UK) for experimental support. We also thank Amanda Hopes and Thomas Mock (University of East Anglia, UK) for guidance with the *T. pseudonana* transformation.

AUTHOR CONTRIBUTIONS

K.E.H., G.L.W., and A.P.R. designed the experiments; K.E.H., E.H., J.D., J.C.-O., M.M.A.-F., F.H.K., and L.A.-M. conducted the experiments. K.E.H., A.P.R., and J.C.-O. analyzed the data. K.E.H. wrote the paper with input from G.L.W., J.C.-O., C.B., and A.P.R.

DECLARATION OF INTERESTS

The authors declare no competing interests.

Received: August 7, 2020
Revised: October 26, 2020
Accepted: November 30, 2020
Published: December 28, 2020

REFERENCES

1. Field, C.B., Behrenfeld, M.J., Randerson, J.T., and Falkowski, P. (1998). Primary production of the biosphere: integrating terrestrial and oceanic components. Science *281*, 237–240.
2. Jin, X., Gruber, N., Dune, J.P., Sarmiento, J.L., and Armstrong, R.A. (2006). Diagnosing the contribution of phytoplankton functional groups to the production and export of particulate organic carbon, $CaCO_3$, and opal from global nutrient and alkalinity distributions. Global Biogeochem. Cycles *20*, GB2015.
3. Buchan, A., LeCleir, G.R., Gulvik, C.A., and González, J.M. (2014). Master recyclers: features and functions of bacteria associated with phytoplankton blooms. Nat. Rev. Microbiol. *12*, 686–698.
4. Kämpf, J., and Chapman, P. (2016). The Functioning of Coastal Upwelling Systems of the World (Springer International), pp. 31–65.
5. Jordan, M.B., and Joint, I. (1998). Seasonal variation in nitrate:phosphate ratios in the English Channel 1923–1987. Estuar. Coast. Shelf Sci. *46*, 157–164.
6. Litchman, E. (2007). Resource competition and the ecological success of phytoplankton. In Evolution of Primary Producers in the Sea, P.G. Falkowski, and A.H. Knoll, eds. (Elsevier), pp. 351–375.
7. Dyhrman, S.T., Ammerman, J.W., and Van Mooy, B.A.S. (2007). Microbes and the marine phosphorus cycle. Oceanography *20*, 110–116.
8. Thingstad, T.F., Zweifel, U.L., and Rassoulzadegan, F. (1998). P limitation of heterotrophic bacteria and phytoplankton in the northwest Mediterranean. Limnol. Oceanogr. *43*, 88–94.
9. Wu, J., Sunda, W., Boyle, E.A., and Karl, D.M. (2000). Phosphate depletion in the western North Atlantic Ocean. Science *289*, 759–762.
10. Ly, J., Philippart, C.J.M., and Kromkamp, J.C. (2014). Phosphorus limitation during a phytoplankton spring bloom in the western Dutch Wadden Sea. J. Sea Res. *88*, 109–120.
11. Burson, A., Stomp, M., Akil, L., Brussaard, C.P.D., and Huisman, J. (2016). Unbalanced reduction of nutrient loads has created an offshore gradient from phosphorus to nitrogen limitation in the North Sea. Limnol. Oceanogr. *61*, 869–888.
12. Alexander, H., Jenkins, B.D., Rynearson, T.A., and Dyhrman, S.T. (2015). Metatranscriptome analyses indicate resource partitioning between diatoms in the field. Proc. Natl. Acad. Sci. USA *112*, E2182–E2190.
13. Wurch, L.L., Alexander, H., Frischkorn, K.R., Haley, S.T., Gobler, C.J., and Dyhrman, S.T. (2019). Transcriptional shifts highlight the role of nutrients in harmful brown tide dynamics. Front. Microbiol. *10*, 136.
14. Paytan, A., and McLaughlin, K. (2007). The oceanic phosphorus cycle. Chem. Rev. *107*, 563–576.
15. V Bondoc, K.G., Lembke, C., Vyverman, W., and Pohnert, G. (2019). Selective chemoattraction of the benthic diatom *Seminavis robusta* to phosphate but not to inorganic nitrogen sources contributes to biofilm structuring. MicrobiologyOpen *8*, e00694.
16. Cruz de Carvalho, M.H., Sun, H.-X., Bowler, C., and Chua, N.-H. (2016). Noncoding and coding transcriptome responses of a marine diatom to phosphate fluctuations. New Phytol. *210*, 497–510.
17. Dyhrman, S.T., Jenkins, B.D., Rynearson, T.A., Saito, M.A., Mercier, M.L., Alexander, H., et al. (2012). The transcriptome and proteome of the diatom *Thalassiosira pseudonana* reveal a diverse phosphorus stress response. PLoS ONE *7*, e33768.
18. Alipanah, L., Winge, P., Rohloff, J., Najafi, J., Brembu, T., and Bones, A.M. (2018). Molecular adaptations to phosphorus deprivation and comparison with nitrogen deprivation responses in the diatom *Phaeodactylum tricornutum*. PLoS ONE *13*, e0193335.
19. Yang, Z.-K., Zheng, J.-W., Niu, Y.-F., Yang, W.-D., Liu, J.-S., and Li, H.-Y. (2014). Systems-level analysis of the metabolic responses of the diatom *Phaeodactylum tricornutum* to phosphorus stress. Environ. Microbiol. *16*, 1793–1807.
20. Dyhrman, S.T. (2016). Nutrients and their acquisition: phosphorus physiology in microalgae. In The Physiology of Microalgae, M. Borowitzka, J. Beardall, and J. Raven, eds. (Springer International), pp. 155–183.
21. Lin, H.-Y., Shih, C.-Y., Liu, H.-C., Chang, J., Chen, Y.-L., Chen, Y.-R., et al. (2013). Identification and characterization of an extracellular alkaline phosphatase in the marine diatom *Phaeodactylum tricornutum*. Mar. Biotechnol. (NY) *15*, 425–436.

22. Van Mooy, B.A.S., Fredricks, H.F., Pedler, B.E., Dyhrman, S.T., Karl, D.M., Koblízek, M., Lomas, M.W., Mincer, T.J., Moore, L.R., Moutin, T., et al. (2009). Phytoplankton in the ocean use non-phosphorus lipids in response to phosphorus scarcity. Nature *458*, 69–72.

23. Martin, P., Van Mooy, B.A.S., Heithoff, A., and Dyhrman, S.T. (2011). Phosphorus supply drives rapid turnover of membrane phospholipids in the diatom *Thalassiosira pseudonana*. ISME J. *5*, 1057–1060.

24. Wykoff, D.D., Grossman, A.R., Weeks, D.P., Usuda, H., and Shimogawara, K. (1999). Psr1, a nuclear localized protein that regulates phosphorus metabolism in Chlamydomonas. Proc. Natl. Acad. Sci. USA *96*, 15336–15341.

25. Kumar Sharma, A., Mühlroth, A., Jouhet, J., Maréchal, E., Alipanah, L., Kissen, R., Brembu, T., Bones, A.M., and Winge, P. (2020). The Myb-like transcription factor phosphorus starvation response (PtPSR) controls conditional P acquisition and remodelling in marine microalgae. New Phytol. *225*, 2380–2395.

26. Liu, K.H., Niu, Y., Konishi, M., Wu, Y., Du, H., Sun Chung, H., Li, L., Boudsocq, M., McCormack, M., Maekawa, S., et al. (2017). Discovery of nitrate-CPK-NLP signalling in central nutrient-growth networks. Nature *545*, 311–316.

27. Riveras, E., Alvarez, J.M., Vidal, E.A., Oses, C., Vega, A., and Gutiérrez, R.A. (2015). The calcium ion is a second messenger in the nitrate signaling pathway of Arabidopsis. Plant Physiol. *169*, 1397–1404.

28. Behera, S., Long, Y., Schmitz-Thom, I., Wang, X.-P., Zhang, C., Li, H., Steinhorst, L., Manishankar, P., Ren, X.-L., Offenborn, J.N., et al. (2017). Two spatially and temporally distinct Ca^{2+} signals convey Arabidopsis thaliana responses to K^+ deficiency. New Phytol. *213*, 739–750.

29. Falciatore, A., d'Alcalà, M.R., Croot, P., and Bowler, C. (2000). Perception of environmental signals by a marine diatom. Science *288*, 2363–2366.

30. Vardi, A., Formiggini, F., Casotti, R., De Martino, A., Ribalet, F., Miralto, A., and Bowler, C. (2006). A stress surveillance system based on calcium and nitric oxide in marine diatoms. PLoS Biol. *4*, e60.

31. Helliwell, K.E., Chrachri, A., Koester, J.A., Wharam, S., Verret, F., Taylor, A.R., et al. (2019). Alternative mechanisms for fast $Na^+/Ca2^+$ signaling in eukaryotes via a novel class of single-domain voltage-gated channels. Curr. Biol. *29*, 1503–1511.e6.

32. Zhao, Y., Araki, S., Wu, J., Teramoto, T., Chang, Y.-F., Nakano, M., Abdelfattah, A.S., Fujiwara, M., Ishihara, T., Nagai, T., and Campbell, R.E. (2011). An expanded palette of genetically encoded Ca^{2+} indicators. Science *333*, 1888–1891.

33. Costa, A., Navazio, L., and Szabo, I. (2018). The contribution of organelles to plant intracellular Calcium signalling. J. Exp. Bot. *69*, 4175–4193.

34. Guillard, R.R., and Ryther, J.H. (1962). Studies of marine planktonic diatoms. I. *Cyclotella nana* Hustedt, and *Detonula confervacea* (cleve) Gran. Can. J. Microbiol. *8*, 229–239.

35. Guillard, R.R.L. (1975). Culture of phytoplankton for feeding marine invertebrates. In Culture of Marine Invertebrate Animals, W.L. Smith, and M.H. Chanley, eds. (Springer US), pp. 29–60.

36. Maxwell, K., and Johnson, G.N. (2000). Chlorophyll fluorescence–a practical guide. J. Exp. Bot. *51*, 659–668.

37. Archer, S.D., Cummings, D.G., Llewellyn, C.A., and Fishwick, J.R. (2009). Phytoplankton taxa, irradiance and nutrient availability determine the seasonal cycle of DMSP in temperate shelf seas. Mar. Ecol. Prog. Ser. *394*, 111–124.

38. Björkman, K.M., and Karl, D.M. (2003). Bioavailability of dissolved organic phosphorus in the euphotic zone at Station ALOHA, North Pacific Subtropical Gyre. Limnol. Oceanogr. *48*, 1049–1057.

39. Karl, D.M., and Björkman, K.M. (2002). Dynamics of DOP. In Biogeochemistry of Marine Dissolved Organic Matter, D.A. Hansell, and C.A. Carlson, eds. (Academic), pp. 249–366.

40. Kolowith, L.C., Ingall, E.D., and Benner, R. (2001). Composition and cycling of marine organic phosphorus. Limnol. Oceanogr. *46*, 309–320.

41. Tanaka, K., Choi, J., Cao, Y., and Stacey, G. (2014). Extracellular ATP acts as a damage-associated molecular pattern (DAMP) signal in plants. Front. Plant Sci. *5*, 446.

42. Tang, W., Brady, S.R., Sun, Y., Muday, G.K., and Roux, S.J. (2003). Extracellular ATP inhibits root gravitropism at concentrations that inhibit polar auxin transport. Plant Physiol. *131*, 147–154.

43. Diaz, J.M., Holland, A., Sanders, J.G., Bulski, K., Mollett, D., Chou, C.-W., Phillips, D., Tang, Y., and Duhamel, S. (2018). Dissolved organic phosphorus utilization by phytoplankton reveals preferential degradation of polyphosphates over phosphomonoesters. Front. Mar. Sci. *5*, 380.

44. Flynn, K.J., Öpik, H., and Syrett, P.J. (1986). Localization of the alkaline phosphatase and 5¢-nucleotidase activities of the diatom *Phaeodactylum tricornutum*. J. Gen. Microbiol. *132*, 289–298.

45. Kaczmarska, I., Beaton, M., Benoit, A.C., and Medlin, L.K. (2006). Molecular phylogeny of selected members of the order Thalassiosirales (Bacillariophyta) and evolution of the fultoportula. J. Phycol. *42*, 121–138.

46. Falciatore, A., Jaubert, M., Bouly, J.P., Bailleul, B., and Mock, T. (2020). Diatom molecular research comes of age: Model species for studying phytoplankton biology and diversity. Plant Cell *32*, 547–572.

47. Lohse, M., Nagel, A., Herter, T., May, P., Schroda, M., Zrenner, R., Tohge, T., Fernie, A.R., Stitt, M., and Usadel, B. (2014). Mercator: a fast and simple web server for genome scale functional annotation of plant sequence data. Plant Cell Environ. *37*, 1250–1258.

48. Wurch, L.L., Bertrand, E.M., Saito, M.A., Van Mooy, B.A.S., and Dyhrman, S.T. (2011). Proteome changes driven by phosphorus deficiency and recovery in the brown tide-forming alga *Aureococcus anophagefferens*. PLoS ONE *6*, e28949.

49. Balamurugan, S., Wang, X., Wang, H.-L., An, C.-J., Li, H., Li, D.-W., Yang, W.-D., Liu, J.-S., and Li, H.-Y. (2017). Occurrence of plastidial triacylglycerol synthesis and the potential regulatory role of AGPAT in the model diatom *Phaeodactylum tricornutum*. Biotechnol. Biofuels *10*, 97.

50. Verret, F., Wheeler, G., Taylor, A.R., Farnham, G., and Brownlee, C. (2010). Calcium channels in photosynthetic eukaryotes: implications for evolution of calcium-based signalling. New Phytol. *187*, 23–43.

51. Vincent, F., and Duncton, M.A. (2011). TRPV4 agonists and antagonists. Curr. Top. Med. Chem. *11*, 2216–2226.

52. Cáceres, C., Spatharis, S., Kaiserli, E., Smeti, E., Flowers, H., and Bonachela, J.A. (2019). Temporal phosphate gradients reveal diverse acclimation responses in phytoplankton phosphate uptake. ISME J. *13*, 2834–2845.

53. Sabir, J.S.M., Theriot, E.C., Manning, S.R., Al-Malki, A.L., Khiyami, M.A., Al-Ghamdi, A.K., et al. (2018). Phylogenetic analysis and a review of the history of the accidental phytoplankter, *Phaeodactylum tricornutum* Bohlin (Bacillariophyta). PLoS ONE *13*, e0196744.

54. Lin, H.-Y., Yen, S.-C., Kuo, P.-C., Chung, C.-Y., Yeh, K.-L., Huang, C.-H., Chang, J., and Lin, H.-J. (2017). Alkaline phosphatase promoter as an efficient driving element for exogenic recombinant in the marine diatom *Phaeodactylum tricornutum*. Algal Res. *23*, 58–65.

55. Du, X., and Peterson, W.T. (2014). Seasonal cycle of phytoplankton community composition in the coastal upwelling system off Central Oregon in 2009. Estuaries Coasts *37*, 299–311.

56. Vidal, T., Calado, A.J., Moita, M.T., and Cunha, M.R. (2017). Phytoplankton dynamics in relation to seasonal variability and upwelling and relaxation patterns at the mouth of Ria de Aveiro (West Iberian Margin) over a four-year period. PLoS ONE *12*, e0177237.

57. Smyth, T.J., Fishwick, J.R., AL-Moosawi, L., Cummings, D.G., Harris, C., Kitidis, V., Rees, A., Martinez-Vicente, V., and Woodward, E.M.S. (2010). A broad spatio-temporal view of the Western English Channel observatory. J. Plankton Res. *32*, 585–601.

58. McCarthy, J.K., Smith, S.R., McCrow, J.P., Tan, M., Zheng, H., Beeri, K., Roth, R., Lichtle, C., Goodenough, U., Bowler, C.P., et al. (2017). Nitrate reductase knockout uncouples nitrate transport from nitrate assimilation and drives repartitioning of carbon flux in a model pennate diatom. Plant Cell *29*, 2047–2070.

59. Smith, S.R., Dupont, C.L., McCarthy, J.K., Broddrick, J.T., Oborník, M., Horák, A., Füssy, Z., Cihlář, J., Kleessen, S., Zheng, H., et al. (2019). Evolution and regulation of nitrogen flux through compartmentalized metabolic networks in a marine diatom. Nat. Commun. *10*, 4552.

60. Downes-Tettmar, N., Rowland, S., Widdicombe, C., Woodward, M., and Llewellyn, C. (2013). Seasonal variation in *Pseudo-nitzschia* spp. and domoic acid in the Western English Channel. Cont. Shelf Res. *53*, 40–49.

61. Watson, G.M.F., Scanlan, D.J., and Mann, N.H. (1996). Characterization of the genes encoding a phosphate-regulated two component sensory system in the marine cyanobacterium *Synechococcus* sp. WH7803. FEMS Microbiol. Lett. *142*, 105–109.

62. Wanner, B.L. (1996). Phosphorus assimilation and control of the phosphate regulon. In Escherichia coli and *Salmonella typhimurium* Cellular and Molecular Biology, F.C. Neidhardt, ed. (American Society for Microbiology).

63. Matthus, E., Wilkins, K.A., Swarbreck, S.M., Doddrell, N.H., Doccula, F.G., Costa, A., and Davies, J.M. (2019). Phosphate starvation alters abiotic-stress-induced cytosolic free calcium increases in roots. Plant Physiol. *179*, 1754–1767.

64. Rayko, E., Maumus, F., Maheswari, U., Jabbari, K., and Bowler, C. (2010). Transcription factor families inferred from genome sequences of photosynthetic stramenopiles. New Phytol. *188*, 52–66.

65. Perez-Riverol, Y., Csordas, A., Bai, J., Bernal-Llinares, M., Hewapathirana, S., Kundu, D.J., Inuganti, A., Griss, J., Mayer, G., Eisenacher, M., et al. (2019). The PRIDE database and related tools and resources in 2019: improving support for quantification data. Nucleic Acids Res. *47* (D1), D442–D450.

66. Poulsen, N., Chesley, P.M., and Kröger, N. (2006). Molecular genetic manipulation of the diatom *Thalassiosira pseudonana* (Bacillariophyceae). J. Phycol. *42*, 1059–1065.

67. Schneider, C.A., Rasband, W.S., and Eliceiri, K.W. (2012). NIH Image to ImageJ: 25 years of image analysis. Nat. Methods *9*, 671–675.

68. Hopes, A., Nekrasov, V., Kamoun, S., and Mock, T. (2016). Editing of the urease gene by CRISPR-Cas in the diatom *Thalassiosira pseudonana*. Plant Methods *12*, 49.

69. Christie-Oleza, J.A., and Armengaud, J. (2010). In-depth analysis of exoproteomes from marine bacteria by shotgun liquid chromatography-tandem mass spectrometry: the Ruegeria pomeroyi DSS-3 case-study. Mar. Drugs *8*, 2223–2239.

70. Kaur, A., Hernandez-Fernaud, J.R., Aguilo-Ferretjans, M.D.M., Wellington, E.M., and Christie-Oleza, J.A. (2018). 100 Days of marine Synechococcus-Ruegeria pomeroyi interaction: a detailed analysis of the exoproteome. Environ. Microbiol. *20*, 785–799.

71. Christie-Oleza, J.A., Scanlan, D.J., and Armengaud, J. (2015). "You produce while I clean up", a strategy revealed by exoproteomics during Synechococcus-Roseobacter interactions. Proteomics *15*, 3454–3462.

72. Cox, J., and Mann, M. (2008). MaxQuant enables high peptide identification rates, individualized p.p.b.-range mass accuracies and proteome-wide protein quantification. Nat. Biotechnol. *26*, 1367–1372.

73. Cox, J., Hein, M.Y., Luber, C.A., Paron, I., Nagaraj, N., and Mann, M. (2014). Accurate proteome-wide label-free quantification by delayed normalization and maximal peptide ratio extraction, termed MaxLFQ. Mol. Cell. Proteomics *13*, 2513–2526.

74. Tyanova, S., Temu, T., Sinitcyn, P., Carlson, A., Hein, M.Y., Geiger, T., Mann, M., and Cox, J. (2016). The Perseus computational platform for comprehensive analysis of (prote)omics data. Nat. Methods *13*, 731–740.

75. Ritchie, R.J. (2008). Universal chlorophyll equations for estimating chlorophylls *a*, *b*, *c*, and *d* and total chlorophylls in natural assemblages of photosynthetic organisms using acetone, methanol, or ethanol solvents. Photosynthetica *46*, 115–126.

76. Ruban, A.V. (2016). Nonphotochemical chlorophyll fluorescence quenching: mechanism and effectiveness in protecting plants from photodamage. Plant Physiol. *170*, 1903–1916.

77. Dugdale, R.C., and Goering, J.J. (1967). Uptake of new and regenerated forms of nitrogen in primary productivity. Limnol. Oceanogr. *12*, 196–206.

78. Rees, A., Woodward, M., and Joint, I. (1999). Measurement of nitrate and ammonium uptake at ambient concentrations in oligotrophic waters of the North-East Atlantic Ocean. Mar. Ecol. Prog. Ser. *187*, 295–300.

STAR★METHODS

KEY RESOURCES TABLE

REAGENT or RESOURCE	SOURCE	IDENTIFIER
Chemicals, Peptides, and Recombinant Proteins		
Monosodium dihydrogen orthophosphate (NaH_2PO_4)	Sigma-Aldrich	Cat. No. S3139
Adenosine triphosphate (ATP)	Thermo Fisher	Cat. No. R0441
D-glucose-6-phosphate (G_6P)	Sigma-Aldrich	Cat. No. G7879
Pentasodium tripolyphosphate hexahydrate	Sigma-Aldrich	Cat. No. T5633
bis-(*p*-nitrophenyl)phosphate (b-NPP)	Sigma-Aldrich	Cat. No. N3002
Adenosine-5′-(3-thiotriphosphate) (ATP-γ-S)	Jena-Bioscience	Cat. No. NU-406-5
Sodium nitrate-15N ($\geq$ 98 atom% ^{15}N, $\geq$ 99%)	Sigma-Aldrich	Cat. No. 364606
Nile Red	Sigma-Aldrich	Cat. No. R2751
cOmplete™ protease inhibitor cocktail	Merck	Cat. No. 11697498001
Ruthenium Red	Sigma-Aldrich	Cat. No. R2751
Verapamil hydrochloride	Tocris	Cat. No. 0654
Spermidine	Sigma-Aldrich	Cat. No. S2626
Tungsten M-10 Microcarriers	BioRad	Cat. No. 1652266
Nourseothricin	Jena BioScience	Cat. No. AB-102L
Poly-L-lysine	Sigma Aldrich	CAS 25988-63-0
Critical Commercial Assays		
Pierce BCA Protein Assay kit	Thermo Fisher Scientific	Cat. No. 23225
Deposited Data		
Proteomics data	ProteomeXchange Consortium, PRIDE[65].	PRIDE: PXD022586
Experimental Models: Organisms/Strains		
Phaeodactylum tricornutum (strain CCAP1055/1)	Culture Collection of Algae & Protozoa	https://www.ccap.ac.uk/
Phaeodactylum tricornutum (strain CCAP1055/1), PtR1 strain	[31]	N/A
Thalassiosira pseudonana (strain CCMP1335)	National Centre for Marine Algae and Microbiota	https://ncma.bigelow.org/
Recombinant DNA		
pTp-FCP/NAT vector	[66]	N/A
pTp-FCP/R-GECO1	This study.	N/A
Software and Algorithms		
NIS-ELEMENTS v.3.1 software	Nikon Instruments Europe B.V.	https://www.microscope.healthcare.nikon.com/en_EU/products/software/nis-elements/nis-elements-advanced-research
ImageJ	[67]	N/A
SigmaPlot (version 11)	Sigmaplot	http://www.sigmaplot.co.uk/
Other		
35 mm glass-bottomed dishes	IBL Baustoff + Labor GmbH	D35-10-0-N
PDS-1000/He Particle Delivery System	Bio-Rad, Hercules, CA, USA	N/A
1350 PSI Rupture Disks	BioRad	1652330
He Macrocarriers	BioRad	165-2257

RESOURCE AVAILABILITY

Lead Contact

Further information and requests for resources and reagents should be directed to and will be fulfilled by the Lead Contact, Katherine Helliwell (Katherine.helliwell@mba.ac.uk; k.helliwell@exeter.ac.uk).

Materials Availability

Strains and plasmids generated in this study are available upon request.

Data and Code availability

The mass spectrometry proteomics data have been deposited to the ProteomeXchange Consortium via the PRIDE[65] partner repository with the dataset identifier PRIDE: PXD022586.

EXPERIMENTAL MODEL AND SUBJECT DETAILS

Strains and cultivation of *P. tricornutum* and *T. pseudonana*

P. tricornutum strain CCAP1055/1 was obtained from the Culture Collection of Algae and Protozoa (SAMS limited, Scottish Marine Institute, Oban, UK). *T. pseudonana* (strain CCMP1335) was kindly donated by Thomas Mock (University of East Anglia, UK). The transgenic line of *P. tricornutum* expressing R-GECO1[32] (PtR1) was generated as described by Helliwell et al., (2019)[31]. *P. tricornutum* and *T. pseudonana* cultures were maintained in natural seawater (NSW) supplemented with f/2 nutrients[34,35], with 100 μM $Na_2SiO_3.5H_2O$ (but not vitamins for *P. tricornutum*) unless stated otherwise, and illuminated with 50-80 μmol m^{-2} s^{-1} light, on a 16:8 h light:dark cycle at 18°C. For experiments with artificial seawater (ASW), the following recipe was used: 450 mM NaCl, 30 mM $MgCl_2$, 16 mM $MgSO_4$, 8 mM KCl, 10 mM $CaCl_2$, 2 mM $NaHCO_3$, and 97 μM H_3BO_3), with f/2 nutrients + Si (but not vitamins for *P. tricornutum*). For the Ca^{2+} free (-Ca^{2+}) ASW medium used for experiments displayed in Figure 6A, the same recipe for ASW was used, but without 10 mM $CaCl_2$ (and 200 μM EGTA was added). For all physiology and signaling experiments *P. tricornutum* cultures were inoculated to a cell density of 3 × 10^4 cells ml^{-1} in liquid culture.

For the nutrient (N, P, f/2 metals) limitation treatments for nutrient resupply experiments described in Figure 1C, cells were grown in f/2 medium made up with NSW, but with concentrations of nitrate or phosphate reduced to one twentieth of those typically found in standard f/2 medium (44 μM and 1.8 μM of nitrate and phosphate, respectively)[34,35], and no f/2 metals for the trace metal limitation treatment (Met).

METHOD DETAILS

Generation of *T. pseudonana* R-GECO1 constructs

To generate the *T. pseudonana* R-GECO1 construct (pTp-fcp/R-GECO1), we synthesized (GenScript, Piscataway, NJ) the 1251 bp coding sequence for R-GECO1 (accession AEO16866.1), and sub-cloned it into the pTp-fcp/nat vector[66], using the restriction sites SphI and NotI. This construct was then co-transformed into WT *T. pseudonana* (CCMP1335), with the pTp-fcp/nat plasmid[66] conferring resistance to nourseothricin (NTC), via biolistic transformation.

Biolistic transformation of *T. pseudonana*

T. pseudonana was co-transformed via biolistic particle bombardment, as previously described by Hopes et al., (2016)[68]. Briefly, 50 μL of 60 mg/μl M10 Bio-Rad tungsten microcarriers were washed three times with Milli-Q water (via repeated centrifugation (at 10,000 rpm, for 15 s, at 21°C), and resuspension steps). The tungsten particles were then resuspended in 50 μl of Milli-Q water, and combined with plasmid DNA (including 5 μl each of 1 μg/μl pTp-fcp/R-GECO1 and 1 μg/μl Tp-fcp/nat), followed by 50 μl of $CaCl_2$ 2.5 M and 20 μL of 0.1 M spermidine, while continuously vortexing. Particles were then washed with 250 μl of 100% ethanol and collected via centrifugation (10,000 rpm, for 15 s, at 21°C). The resulting pellet was then resuspended in 50 μ 100% ethanol and transferred onto a macrocarrier disk, and left to dry.

A total of 5 × 10^7 *T. pseudonana* cells were harvested in mid-exponential growth phase via centrifugation (4,000 rpm, 10 mins, at 21°C), resuspended in 100 μl of f/2 medium (made up with 50% diluted NSW), and transferred onto a 47 mm/0.2 μm filter. The filter paper was then placed on the center of a 50% salinity f/2 medium plate containing 1.8% agar without antibiotics and set to incubate for 30 mins.

Biolistic delivery was carried out with a 1350 psi rupture disk positioned at a 7 cm distance from the plate. Following a 24 h recovery phase under standard growth conditions, cells were gently rinsed from the filter paper in 25 ml of ½ salinity f/2 medium. The cells were then spread on 2-3 selection plates (50% salinity f/2 medium 0.8% agar + 300 μg/ml NTC). Dark-brown colonies were transferred into a 24-well plate containing standard f/2 medium and NTC (300 μg/ml).

Epifluorescence imaging in *P. tricornutum* and *T. pseudonana*

P. tricornutum and *T. pseudonana* cells grown in standard liquid culture for four days were placed in a 35 mm glass-bottomed dish (*In Vitro* Scientific, Sunnyvale, CA, USA) coated with 0.01% poly-L-lysine (Sigma-Aldrich, St Louis, MO, USA). Cells adhered to the

bottom of the dish were imaged at 20°C using epifluorescence microscopy with a Nikon Eclipse Ti microscope with a 100 × , 1.30 NA oil immersion objective and detection with a Photometrics Evolve EM-CCD camera (Photometrics, Tucson, AZ, USA). Excitation of R-GECO1 (PtR1 and TpR1) cells was performed using a pE2 excitation system (CoolLED, Andover, UK) with 530-555 nm excitation and 575-630 nm emission filters. Images were captured using NIS-ELEMENTS v.3.1 software (Nikon, Japan) with a 300 ms camera exposure (frame rate of 3.33 frames s^{-1}). Images were processed using NIS-ELEMENTS v.3.1 software. The mean fluorescence intensity within a region of interest (ROI) over time was measured for each cell by drawing an ROI encompassing the whole cell. Change in fluorescence intensity of R-GECO1 was then calculated by normalizing each frame by the initial value (F/F_0).

During imaging, cells were continuously perfused with natural seawater (3 ml min^{-1}). The P resupply treatments were delivered by switching the perfusion from f/2 medium without phosphate (NaH_2PO_4) to f/2 medium with phosphate (typically 36 μM, except in Figure 2A for the phosphate dose experiment), unless otherwise stated. Cells exposed to phosphate resupply treatments in the absence of Ca^{2+} were perfused with at least 20 ml Ca^{2+} free ASW medium (amended with 200 μM EGTA) in order to minimize residual Ca^{2+} from the ASW growth medium. The same set-up was used for hypo-osmotic shock experiments, except the perfusion was switched from undiluted to diluted NSW.

The epifluorescence images of the TpR1 cell displayed in Figure 3A, were acquired using a DMi8 Inverted Microscope with a DFC700 T color camera (Leica Microsystems, Milton Keynes, UK), with a 63 × 1.40 oil immersion objective. Excitation at 543 nm and emission at 565-615 nm was used for R-GECO1 fluorescence. For chlorophyll fluorescence the excitation wavelength was 633 nm and emission was detected at 650-710 nm. Given the heterogeneity of R-GECO1 fluorescence in the TpR1, we defined cells exhibiting a baseline R-GECO1 fluorescence intensity of at least 2.8 fold greater than background levels, as positive for R-GECO1 fluorescence. Using this threshold value we estimated that 57% of the population (grown under standard nutrient replete conditions) exhibited R-GECO1 fluorescence. Compared to P replete conditions, basal RGECO-1 fluorescence was much lower in the P-limited conditions, and so it was not possible to distinguish between cells with high versus no/low R-GECO1 expression. Hence we reported the proportion of cells exhibiting a Ca^{2+} elevation, out of the total population of cells examined, in response to the phosphate/osmotic treatments.

Treatment with pharmacological inhibitors for Ca^{2+}-signaling experiments

Prior to phosphate resupply and/or hypo-osmotic shock treatments, cells were bathed in seawater containing verapamil (5 μM), Ruthenium Red (RuR, 5 μM or 10 μM) for 5 mins in glass-bottomed dishes (stock solutions for these chemicals were made up in ddH_2O). Experimental treatments switching from medium containing no phosphate to 36 μM phosphate (or to diluted seawater in the case of the hypo-osmotic shock experiments) without the pharmacological agents were then delivered, as outlined above.

Protein preparation for shotgun proteomics

$P_{replete}$, $P_{limited}$, and $P_{resupply}$ treatment cultures were inoculated with PtR1 cells to a cell density of 3×10^4 cells ml^{-1} and incubated in standard growth conditions for four days. We added 36 μM of phosphate to the $P_{resupply}$ cultures and incubated all cultures for an additional four h at 18°C. Cells from 15 ml of culture were harvested by centrifugation (4000 g at 4°C for 5 mins). Supernatants were removed and cell pellets flash-frozen until further analysis. Cell pellets were then dissolved in 100 μl of 1 x LDS loading buffer (Invitrogen, USA) and given three cycles of 5 min sonications (Branson 2510 Ultrasonic water bath), 10 s of vortex and 5 min incubations at 95°C. Thirty μl of the lysate was loaded immediately onto a precast 10% Tris-Bis NuPAGE gel (Invitrogen, USA) using 1 x MOPS solution (Invitrogen, USA) as the running buffer. SDS-PAGE was performed for a short gel migration (5 mm of migration into the gel). Polyacrylamide gel bands containing the cellular proteomes were excised and standard in-gel reduction with dithiothreitol and alkylation with iodoacetamide was performed prior to trypsin (Roche, Switzerland) proteolysis[69]. The resulting tryptic peptide mixture was extracted from the polyacrylamide gel bands and prepared for mass spectrometry as previously described[70].

NanoLC-MS/MS and data analysis of the proteomes

Samples were analyzed by nanoLC-ESI-MS/MS using an Ultimate 2000 LC system (120 minute LC separation on a 25 cm column; Dionex-LC Packings) coupled to an Orbitrap Fusion mass spectrometer (Thermo-Scientific, USA), using LC conditions and MS settings as described previously[71]. Raw MS/MS files were processed with MaxQuant version 1.5.3.30[72] for protein identification and LFQ quantification[73], using default parameters, match between runs and *P. tricornutum* strain CCAP 1055/1 protein database (Ref. UP000000759) obtained from UniProt. The comparative proteomic analysis between samples (i.e., data filtering and processing, as well as two-sample Student's t tests and fold changes) was carried out using Perseus version 1.5.5.3[74] following the pipeline described previously[70], but including a stringent rule where only proteins confidently detected in all three biological replicates of at least one condition were considered. The full list of detected proteins is available in Data S1.

Biochemical analyses

Total protein extraction and quantification

For total protein analyses, 2 ml of cells were spun down for 2 mins at 13,000 g at 20°C, the supernatant removed, and pellets flash-frozen in liquid nitrogen. Cell pellets were then re-suspended in 50-200 μl (according to original cell density) of protein extraction buffer (comprising of 2% SDS, 5 mM tris-HCL pH 6.8, cOmplete™ protease inhibitor cocktail (1 tablet per 50 ml of extraction buffer), and sonicated for 3 mins in a sonication bath with ice. Total protein was then quantified using a Pierce BCA Protein Assay kit (Thermo Fisher Scientific), according to manufacturer's instructions.

Chlorophyll quantification

To measure total chlorophyll concentrations a 2 ml aliquot of *P. tricornutum* cells was centrifuged for 2 mins at 13,000 g at 21°C, the supernatant discarded and cell pelleted re-suspended in 1 ml ethanol. Chlorophyll pigments were extracted by vortexing for 2 mins, followed by centrifugation at 13,000 g for 2 mins at 21°C. Optical density of the supernatant was then measured at 652, 665, and 750 nm, and the equations from Ritchie et al., (2008)[75] applied to calculate chlorophyll *a* concentration per cell.

Neutral lipid staining and quantification

One ml of cells were stained with 1 μl of 25 μg ml^{-1} Nile Red dissolved in DMSO. Fluorescence was then measured in a CLARIOstar plate reader (BMG LABTECH) using the AlexaFluor532 pre-setting (excitation/emission settings: 482 ± 16/570-530).

Photo-physiological measurements

Measurements of Fv/Fm and non-photochemical quenching (NPQ) were made on dark-adapted (15 mins) cells using an AquaPen-C device (Photon Systems Instruments). For NPQ measurements, different treatments were diluted to equivalent cell densities prior to quantification (OD_{730} between 0.02-0.03). The predefined NPQ3 setting was used (light duration 200 s, 10 pulses; dark recovery duration 60 s, 2 pulses), with light intensity settings as follows: 450 μmol.m^{-2}.s^{-1} (actinic light), 3000 μmol.m^{-2}.s^{-1} (super-pulse i.e 100%) and 20% for the flash pulse. The NPQ was calculated via the following equation: $(F_m-F_m')/F_m'$ (where F_m is maximum fluorescence measured in dark-adapted state and F_m' maximum fluorescence of samples illuminated with actinic light), as per Ruban et al., (2016)[76]. Values for Φ_{PSII} (QY_{LSS}) were then extracted to calculate electron transport rate (ETR) using the following equation: Φ_{PSII} × photosynthetically active radiation (PAR) × 0.5 (where PAR was 450 μmol photon m^{-2} s^{-1} (actinic light)), according to Maxwell et al., (2000)[36].

Nitrogen uptake experiments

$P_{replete}$, $P_{limited}$, and $P_{resupply}$ treatment cultures were inoculated with PtR1 cells to a cell density of 3 × 10^4 cells ml^{-1} and incubated in standard growth conditions for four days. Sodium nitrate-15N (≥98 atom% ^{15}N, ≥ 99%, Sigma Aldrich, 364606) was added to the cultures (to a concentration 10% of the ambient nitrate)[77], and cells incubated for 1 hour at 18°C. Phosphate (36 μM) was then added to the $P_{resupply}$ cultures. Cells were harvested at each time-point by centrifugation at 4000 g for 10 mins at 4°C, supernatant removed and pellets snap-frozen in liquid nitrogen. Total cellular nitrogen content (μmol N) and incorporation of the ^{15}N label into cellular material (atom%^{15}N) were determined using a stable isotope ratio mass spectrometer coupled to high temperature combustion elemental analyzer (SERCON Ltd)[78].

QUANTIFICATION AND STATISTICAL ANALYSIS

Statistical Analyses

Quantification of data are presented as mean ± standard error of the mean (SEM) with the number (*n*) indicated in the figure legends and where relevant the main text. Statistical analyses were performed using a Student's t test or one-way ANOVA test in SigmaPlot. Statistical differences are represented as p*, < 0.05; **, p < 0.01; ***, p < 0.001.

Data and Software Availability

The accession number for the proteomic datasets in GenBank and sources of plasmids used in this study are given in the Key Resources Table.